Nernst, Seebeck, and Hall effects in the mixed state of $YBa_2Cu_3O_{7-\delta}$ and $Bi_2Sr_2CaCu_2O_{8+x}$ thin films: A comparative study

H.-C. Ri, R. Gross, F. Gollnik, A. Beck, and R. P. Huebener
Lehrstuhl Experimentalphysik II, Universität Tübingen, Morgenstelle 14, D-72076 Tübingen, Germany

P. Wagner and H. Adrian
Institut für Festkörperphysik, Technische Hochschule Darmstadt, Hochschulstrasse 8, D-64289 Darmstadt, Germany
(Received 28 February 1994)

The anisotropy of the high-temperature superconductors has strong impact on their transport properties in the mixed state. We have performed a comparative study of the Nernst, Seebeck, and Hall effects of the anisotropic and extremely anisotropic high-temperature superconductors $YBa_2Cu_3O_{7-\delta}$ and $Bi_2Sr_2CaCu_2O_{8+x}$, respectively. High-quality, c-axis-oriented epitaxial thin films have been used for our study. The temperature and the magnetic-field dependence of the Nernst and Seebeck electric fields were measured both in the mixed state and in the fluctuation regime above the thermodynamic critical temperature. The Seebeck-effect data can be explained well by an extended two-fluid counterflow picture in analogy to the fountain effect in superfluids. From the Nernst-effect data the temperature and magnetic-field dependence of the transport entropy of magnetic-flux lines has been derived. For the magnetic field applied parallel to the c axis of the films, approximately the same value of the transport entropy was found for $YBa_2Cu_3O_{7-\delta}$ and $Bi_2Sr_2CaCu_2O_{8+x}$, showing that the different anisotropy of these materials has little influence on this quantity. From our experimental data in the mixed state and the fluctuation regime well above the mean-field critical temperature, the upper-critical-field slope was derived. For both regimes, $dH_{c2}/dT=-2.4\pm0.2$ and -2.5 ± 0.2 T/K for $YBa_2Cu_3O_{7-\delta}$ and $Bi_2Sr_2CaCu_2O_{8+x}$, corresponding to a Ginzburg-Landau coherence length $\xi_{ab}=14.5$ and 14.2 Å, respectively. The Hall resistivity ρ_{xy} of both materials showed a sign anomaly in the mixed state and scaled with the longitudinal resistivity ρ_{xx} as $\rho_{xy}(T)=K^{-1}\rho_{xx}^{\beta}(T)$ with $\beta\simeq2$ and a magnetic-field-independent coefficient K.

I. INTRODUCTION

In the mixed state the transport properties of the high-temperature superconductors (HTSC's) are dominated by the motion of the vortex structure. One important aspect of the physics of the HTSC's is their layered structure and the associated large anisotropy. In the anisotropic high-temperature cuprates the structure and the dynamics of the flux-line lattice are markedly different from isotropic superconductors. Due to the large anisotropy of HTSC's and with their vortex-pinning energies being comparable to thermal energies, the mixed state of these materials shows interesting phenomena, which have been studied intensively in the last few years. The specific properties of the HTSC's manifest themselves in a distinct broadening of the resistive transition in an applied magnetic field,[1,2] a strongly time-dependent value of the dc magnetization,[3,4] or a considerable frequency and magnetic-field dependence of the ac susceptibility transition.[5–7] The HTSC's also have renewed the theoretical interest in the phenomenology of type-II superconductors. Among the recent results are thermodynamic phases such as the vortex glass[8] or different kinds of vortex liquids,[9] the influence of thermal fluctuations leading to thermal depinning[10] and vortex lattice melting,[9,11,12] the determination of the elastic properties of the vortex lattice in anisotropic superconductors,[11,13,14] and the investigation of classical[15,16] and quantum flux creep.[17]

In the majority of experimental studies of the transport properties in the mixed state of HTSC's the vortex motion due to the Lorentz force of an applied transport or shielding current is investigated. However, there is a further class of experiments, where the thermal diffusion of magnetic-flux lines is caused by the thermal force of an applied temperature gradient. The motion of vortices under the influence of a thermal force results in a pronounced Nernst effect.[18–25] In addition, the Ettingshausen effect as the reciprocal phenomenon has been observed.[26] These thermomagnetic phenomena due to flux motion in the mixed state of the HTSC's allow the determination of important material parameters such as the transport entropy of vortices, the upper critical field slope close to the transition temperature, or the coherence length. We note that also the measurement of the thermal conductivity can be used as a probe of the vortex state.[27]

The influence of the anisotropy on quantities such as the transport entropy of flux lines is still discussed controversially. Whereas for the magnetic field applied parallel to the c axis of the material a similar transport entropy is expected theoretically for $YBa_2Cu_3O_{7-\delta}$ and $Bi_2Sr_2CaCu_2O_{8+x}$, recent measurements suggested that the transport entropy is smaller by a factor of about 10 in

$Bi_2Sr_2CaCu_2O_{8+x}$.[25,28] In our comparative study we performed a careful measurement of the Nernst effect in anisotropic $YBa_2Cu_3O_{7-\delta}$ and extremely anisotropic $Bi_2Sr_2CaCu_2O_{8+x}$ samples both in the mixed state and the fluctuation regime above the mean-field critical temperature. By using the thin-film sample configuration itself as a thermometer the thermoelectric and thermomagnetic effects occurring in the presence of an applied temperature gradient could be measured with high precision.

Beyond the Nernst and Ettingshausen effects, the Seebeck effect and the Peltier effect as the reciprocal phenomenon have been measured recently.[19,22,24,29] These thermoelectric effects are dominated by the thermal diffusion of the quasiparticles under the influence of an applied temperature gradient. Based on an idea of Ginzburg the presence of a pronounced Seebeck effect in the mixed state of a type-II superconductor can be explained by a two-fluid counterflow picture.[30,31] It has been shown recently that the counterflow concept has to be modified for nonzero magnetic fields where the presence of vortices results in a redistribution of the supercurrent in the vicinity of the vortex cores.[32,33] Using epitaxial $YBa_2Cu_3O_{7-\delta}$ and $Bi_2Sr_2CaCu_2O_{8+x}$ films the influence of the anisotropy on the Seebeck effect in the mixed state is studied. The experimental data are compared to the predictions of the modified counterflow concept.

The Hall effect in the mixed state recently has attracted much attention. There are two interesting phenomena that still are discussed actively. First, the Hall coefficient shows a sign anomaly just below the transition temperature.[34–42] Second, there is a striking scaling behavior between the longitudinal resistivity ρ_{xx} and the Hall resistivity ρ_{xy} of the form $\rho_{xy} \propto \rho_{xx}^{\beta}$ with $\beta \sim 2$. This scaling behavior has been observed for different materials.[42–46] Various theoretical explanations have been proposed for these phenomena.[47–53] In our experiments we have studied the Hall effect of the anisotropic and very anisotropic $YBa_2Cu_3O_{7-\delta}$ (YBCO) and $Bi_2Sr_2CaCu_2O_{8+x}$ (BSCCO) superconductors to clarify the role of the anisotropy on the observed peculiarities of the Hall effect in the mixed state. Furthermore, the Hall angles obtained from Lorentz force and thermal force measurements are compared.

After discussing the theoretical background of our experiments in Sec. II and presenting our measuring technique in Sec. III we will show our experimental results on the Nernst, Seebeck, and Hall effects of the anisotropic and extremely anisotropic superconductors $YBa_2Cu_3O_{7-\delta}$ and $Bi_2Sr_2CaCu_2O_{8+x}$ in Sec. IV. The experimental data are compared to the predictions of theoretical models. Fitting the experimental data to the model predictions, important parameters of the investigated materials are derived.

II. THEORETICAL BACKGROUND

In the mixed state of type-II superconductors there are two different species that can transport entropy, namely the quasiparticles and the magnetic-flux lines. Hence, in a temperature gradient a thermal force

$$\mathbf{F}_{\rm th} = -S^* \nabla T \tag{1}$$

acts on both species where S^* is their transport entropy. The thermal force is pointing from the hot to the cold side of the sample. The quasiparticles transport electric charge and their thermal diffusion results in a longitudinal (Seebeck effect) electric field parallel to the applied temperature gradient. In contrast, the flux lines transport magnetic flux and their diffusion results in a transverse (Nernst effect) electric field. In the following we will assume that the temperature gradient is parallel to the x axis and the applied magnetic field parallel to the z axis. In our discussion we initially will not consider the Hall effect of the diffusing species. The Hall effect on the measured Seebeck and Nernst electric field is discussed in Sec. II C. A more detailed discussion has been given recently.[32,33,54]

A. Nernst effect

The Nernst effect is associated with the generation of a transverse electric field E_y in the y direction due to a temperature gradient $\nabla_x T$ applied in the x direction. The Nernst coefficient is defined as

$$\nu = \frac{1}{B_z} \frac{E_y}{\nabla_x T} , \tag{2}$$

where B_z is the magnetic-flux density. The Nernst coefficient is related to the Ettingshausen coefficient ϵ through the Bridgeman relation $T\nu = \epsilon K$, where K is the heat conductivity. In the mixed state the Nernst effect is dominated by the transport of magnetic-flux lines. Since the entropy density close to a vortex is larger than in the superconducting surrounding, there is a thermal force per unit length, $F_{\rm th} = -S_\phi \nabla_x T$, acting on the flux line. Here, S_ϕ is the transport entropy per unit length of flux line. In the absence of pinning the vortices will move (parallel to the driving force). In a steady-state situation the thermal force is balanced by the viscous damping force $F_\eta = -\eta u$, where η is the damping coefficient and u the velocity of the flux lines. According to Josephson[55] the moving vortices generate an electric field $E_y = -u_x B_z$. From the force balance between the thermal driving and the viscous damping force the transport entropy per unit length of flux line is obtained to[21]

$$\frac{E_y}{\nabla_x T} = \frac{\rho_F}{\Phi_0} S_\phi , \tag{3}$$

where ρ_F is the resistivity in the flux motion state.

On the basis of the time-dependent Ginzburg-Landau (GL) theory, Maki[56] and Hu[57] obtained the following theoretical expression for the transport entropy:

$$S_\phi(T) = -\frac{\Phi_0 M(T)}{T} L_D(T) . \tag{4}$$

Here M is the spatially averaged magnetization, Φ_0 the magnetic-flux quantum, and $L_D(T)$ is a numerical function, which is about 1 for T close to T_c. The vortex structure of a type-II superconductor was studied by Abrikosov for the low-field ($H - H_{c1} \ll H_{c1}$) and the

high-field ($H_{c2}-H \ll H_{c2}$) limits based on GL theory.[58] For the high-field limit the magnetization can be expressed as

$$-4\pi M(T)=\frac{H_{c2}(T)-H}{\beta_A(2\kappa^2-1)+1}\ , \tag{5}$$

where κ is the Ginzburg-Landau parameter and $\beta_A=1.16$ for a hexagonal flux-line lattice. According to Eqs. (4) and (5) the transport entropy of a magnetic-flux line is proportional to $H_{c2}-H$, i.e., S_ϕ decreases with increasing magnetic field at constant T. With the approximation of Eq. (5) the transport energy per unit length of flux line, $U_\phi=TS_\phi$, in the high-field limit is given by

$$U_\phi(T)=\frac{\Phi_0}{4\pi}\frac{H_{c2}(T)-H}{\beta_A(2\kappa^2-1)+1}L_D(T)\ . \tag{6}$$

According to GL theory, $dH_{c2}/dT=$const for T close to T_c. Hence, at constant applied magnetic field U_ϕ decreases about linearly with increasing T, since the temperature dependence of L_D is negligible close to T_c. Furthermore, dU_ϕ/dT for different applied magnetic fields should be constant at constant temperature.

Equation (6) suggests that a linear extrapolation of $U_\phi(H)$ or $U_\phi(T)$ should allow to determine $H_{c2}(T)$ or, equivalently, $T_{c2}(H)$. However, we note that the GL approximation for the magnetization is valid only in the high-field regime close to the $H_{c2}(T)$ line. Unfortunately, as discussed below, in this regime the linear $U_\phi(T)$ dependence is not observable due to significant fluctuation contributions. Fluctuation effects play a negligible role in the intermediate-field regime ($H_{c1} \ll H \ll H_{c2}$). In many cases much of the experimental data indeed correspond to fields H well below H_{c2}, where the high-field approximation is not applicable. The invalidity of the high-field GL result manifests itself in a noticeable field dependence of the slope dU_ϕ/dT at constant temperature (see Fig. 5), in contrast to the prediction of Eq. (6).

In the intermediate-field regime the GL equations can no longer be solved in closed form due their nonlinearity. In this field regime the London model[59] has provided a good phenomenological description of extreme type-II superconductors ($\kappa \gg 1$). However, in the London model the depression of the order parameter to zero on the axis of a magnetic flux line is not taken into account resulting in a divergent flux and supercurrent density on the axis of the vortex. Recently, Hao and co-workers[60,61] proposed a theoretical model for the reversible magnetization of type-II superconductors in the whole field regime between H_{c1} and H_{c2}. In calculating the free energy, the kinetic energy and the condensation energy terms arising from the suppression of the order parameter in the vortex core have been included in addition to the supercurrent kinetic energy and the magnetic-field energy. Using the more detailed theoretical analysis of Hao and Clem with the derived expression for the magnetization permits a more accurate determination of $H_{c2}(T)$ from the measured $U_\phi(T)$ dependence than using the linear Abrikosov formula.

1. Effect of anisotropy

Due to their layered structure the high-temperature superconductors are anisotropic. Usually, the anisotropy of the different materials is characterized by their anisotropy ratio $\gamma=\xi_{ab}/\xi_c=\lambda_c/\lambda_{ab}$, which is about 5 for $YBa_2Cu_3O_{7-\delta}$ and more than 150 for $Bi_2Sr_2CaCu_2O_{8+x}$.[62] Here ξ_{ab} and ξ_c are the coherence lengths parallel to the *ab* plane and the *c* axis, λ_c and λ_{ab} are the London penetration depths for currents along the *c* direction and in the *ab* plane, respectively. There are several approaches for the description of the magnetic structure of vortices and the vortex lattice in strongly anisotropic superconductors. In some cases the anisotropic three-dimensional (3D) London theory can be used.[63,64] For the layered high-T_c materials this is possible, if the coherence length ξ_c along the *c* axis is much larger than the spacing s of the two-dimensional Cu-O planes where the superconductivity resides. For most materials $\xi_c < s$ in a broad temperature range and the anisotropic London theory has to be replaced by the Lawrence-Doniach (LD) model.[65–67] This model describes Josephson-coupled superconducting layers of thickness d and stacking periodicity s. In this model the vortex lines are represented by stacks of correlated 2D point vortices residing in the superconducting Cu-O layers connected via Josephson vortices. Since one always considers the transport entropy per unit length of flux line, S_ϕ is some average between the contribution of the point vortices and the connecting Josephson vortices. In the following we will give a qualitative discussion of the impact of the anisotropy on the transport entropy of magnetic-flux lines. Here, we only will consider the case where the magnetic field is applied parallel to the *c* axis.

For a type-II superconductor in the mixed state the free-energy density $\mathcal{F}$ measured relative to the Meissner state is given by

$$\mathcal{F}=\mathcal{F}_{\rm core}+\mathcal{F}_{\rm em}\ . \tag{7}$$

$\mathcal{F}$ is composed of a core part and an electromagnetic part. The core part $\mathcal{F}_{\rm core}$ is given by the sum of the condensation energy and the kinetic energy associated with gradients in the magnitude of the order parameter. The electromagnetic part $\mathcal{F}_{\rm em}$ is composed of the kinetic energy associated with the shielding supercurrent and the magnetic-field energy.

In the high-field regime ($H_{c2}-H \ll H_{c2}$) the core part usually is dominating.[60,61] Furthermore, for a strongly anisotropic high-T_c material the condensation energy and the kinetic energy associated with gradients of the order parameter are concentrated in the 2D Cu-O layers. That is, free-energy density is determined by the core contribution of the point vortices in the 2D Cu-O layers. This suggests that the free-energy density is about the same for different high-T_c materials, which have similar properties within their 2D Cu-O layers and which have a similar distance s between these layers. This is the case for $YBa_2Cu_3O_{7-\delta}$ and $Bi_2Sr_2CaCu_2O_{8+x}$ which have Cu-O double layers with similar spacing. The different coupling strength between the layers has negligible influence on $\mathcal{F}$.

Recently, a similar result was obtained by Clem[68] for magnetic fields $H_{c1} \ll H \ll H_{c2}$. He considered a stack of superconducting layers of thickness d and stacking periodicity s in the extreme limit of zero Josephson-coupling strength. It was assumed that each superconducting layer is isotropic with an intrinsic bulk penetration depth λ_s. The decay length for currents parallel to the layers is given by $\lambda_{\parallel}=\lambda_s(s/d)^{1/2}$. Within this model the free-energy density associated with vortex lines perpendicular to the layers is given by $\mathcal{F}=\mathcal{F}_s(d/s)$, where $\mathcal{F}_s$ is the free-energy density for the isotropic material. For $YBa_2Cu_3O_{7-\delta}$ and $Bi_2Sr_2CaCu_2O_{8+x}$ the ratio d/s is about the same. That is, $\mathcal{F}$ is expected to be about equal for these materials, if $\mathcal{F}_s$ is similar. This is the case for YBCO and BSCCO because of their similar CuO_2 double-layer structure. Note that this model cannot give any information on the effect of the Josephson-coupling strength, since the Josephson coupling was neglected explicitly.

Including the Josephson coupling between the layers, the free-energy density was calculated by Bulaevskii, Ledvij, and Kogan[66,67] based on the LD model for the low- and intermediate-field regime. Taking into account the contribution of the normal core, the free-energy density for $H\|c$ was obtained to

$$\mathcal{F}(B)=\frac{B\Phi_0}{4\pi\mu_0\lambda_{ab}^2}(\ln\kappa+0.5) \quad \text{for } B\to 0 , \tag{8}$$

$$\mathcal{F}(B)=\frac{B\Phi_0}{8\pi\mu_0\lambda_{ab}^2}\left[\ln\frac{\alpha\Phi_0}{2\pi\xi_{ab}^2 B}\right] \quad \text{for } \frac{\Phi_0^2}{4\pi\lambda_{ab}^2}\ll B\ll H_{c2} . \tag{9}$$

Here B is the magnetic induction and α a parameter of the order unity. Note that $\mathcal{F}$ depends only on ξ_{ab} and λ_{ab}. These parameters are about the same for $YBa_2Cu_3O_{7-\delta}$ and $Bi_2Sr_2CaCu_2O_{8+x}$ despite the significantly different anisotropy of these materials. This is caused by the fact that both materials have Cu-O double layers.

The free energy per unit length of flux line is given by $\mathcal{F}/n$, where n is the area density of flux lines. Using the relation $H=1/2(d\mathcal{F}/dB)$ and $M=(B/\mu_0)-H$ it is straightforward to derive the magnetization and, hence, the transport entropy from the expressions for the free-energy density. Summarizing we conclude that the free-energy density for $H\|c$ is determined mainly by the properties of the 2D superconducting layers and is not significantly influenced by the coupling strength between these layers in the entire field regime between H_{c1} and H_{c2}. Therefore, it is expected that the transport energy of magnetic-flux lines is about the same for materials having similar properties in their 2D superconducting layers (e.g., $YBa_2Cu_3O_{7-\delta}$ and $Bi_2Sr_2CaCu_2O_{8+x}$) independent of the degree of Josephson coupling between these layers. As shown below, this expectation agrees well with our experimental observation.

2. *Fluctuation effects*

Apart from a small contribution by the normal charge carriers, according to GL theory the Nernst electric field should disappear for $T\geq T_c(H)$. However, due to the large anisotropy and small coherence length of the HTSC's it is expected that fluctuation effects play an important role over an extended temperature range around T_c. Due to the presence of pronounced fluctuations there is a finite value of the transport entropy also for $T>T_{c2}(H)$. Measurements of the Nernst effect at $T>T_c$ allow the study of these fluctuation effects with great accuracy, since the normal-state contributions are negligible and, hence, no subtraction procedure is required. This is in contrast to the specific heat, electric conductivity, or thermopower.

The study of fluctuation effects in superconductors has a long history with much of the early work focusing on fluctuation effects in zero magnetic field (see, e.g., Ref. 69). Implicit in most of the early work was the assumption that the fluctuations do not interact, i.e., only Gaussian fluctuations were considered. It has been pointed out by Ullah and Dorsey[70,71] that one drastically underestimates the effect of fluctuations, if the Gaussian approximation is used to calculate the properties of type-II superconductors near the mean-field $T_{c2}(H)$ line. This is caused by the fact that fluctuations which are transverse to the applied field have a characteristic length scale given by $l_H=(\Phi_0/2\pi H)^{1/2}$ and, hence, are stiff. The fluctuations in three-dimensional superconductors then become effectively one-dimensional[72] and the superconductor behaves like an array of 1D rods parallel to the applied field with the density of the rods given by the Landau degeneracy factor (H/Φ_0). In this case one expects that interactions between the fluctuations become important in a wider temperature regime around $T_{c2}(H)$.

Based on the time-dependent GL theory the effect of fluctuations on the transport properties of type-II superconductors in magnetic field was calculated by Ullah and Dorsey.[70,71] The interaction between the fluctuations was treated using the Hartree approximation. They derived expressions for the scaling functions of various thermodynamic and transport properties such as the magnetization, electrical conductivity, transport energy, and specific heat. The scaling theory shows that the thermodynamic quantities of high-T_c superconductors exhibit characteristic scaling behavior in the critical fluctuation region in agreement with recent experimental results.[73–76] Their result interpolates smoothly between the high-temperature regime, which is dominated by Gaussian fluctuations, and the low-temperature regime with no intervening divergence. For magnetic fields sufficiently strong that the quasiparticles are limited to be in their lowest Landau level, they obtained the following scaling law for the transport energy:[71,73]

$$U_{\phi}(T,H)=(TH)^m G\left[A\frac{T-T_{c2}(H)}{(TH)^m}\right] . \tag{10}$$

Here G is the scaling function which is not known exactly, but which is universal for all materials. The exponent m depends on the dimensionality of the system. For 2D systems we have $m=\frac{1}{2}$, whereas $m=\frac{2}{3}$ for 3D systems. The scaling functions are valid only in either the two- or three-dimensional limit and not for the general LD mod-

el. The coefficient $A \propto H_{c2}/(T_{c2}\gamma^{2/3}\kappa^{4/3})$ determines the transition width. The large anisotropy, the high GL parameter, and the high critical temperature of HTSC's increase the fluctuation region compared to conventional superconductors. In the regime well below $T_{c2}(H)$ the result obtained for the transport energy from Eq. (10) differs by a factor of $\beta_A/2L_D$ from the mean-field result [Eq. (6)]. This is caused by the fact that the Hartree-Fock approximation does not incorporate the correct vortex lattice structure. By plotting $U_\phi/(TH)^m$ versus $[T-T_{c2}(H)]/(TH)^m$ all data should collapse onto a single curve. The only free parameter in such scaling plot is the mean-field transition temperature $T_{c2}(H)$, which can be derived by fitting the experimental data.

The above scaling law was obtained in the lowest Landau level (LLL) approximation and should be valid only in the high-field limit. For a quasi-2D superconductor in perpendicular magnetic field the high-field limit is equivalent to the condition $|T-T_{c2}(H)| < -6H/(dH_{c2}/dT)$.[77] As an example, for an applied field of 4 T and with $-dH_{c2}/dT \simeq 2$ T/K for $YBa_2Cu_3O_{7-\delta}$, this results in $|T-T_{c2}(H)| < 12$ K. Experimentally the actual range of applicability of the high-field limit was found to be even wider.[73] As pointed out by Ullah and Dorsey[71] the above scaling form in general is not restricted to the high-field case, since the inclusion of higher Landau levels in the Hartree-Fock approximation simply renormalizes the critical temperature and the magnitude of the transport coefficient but not its functional form.

Recently, Tesanovic *et al.*[7,8] obtained an explicit closed expression for the scaling function $G(x)$ for a quasi-2D system using a nonperturbative approach. The derived function is valid everywhere in the critical region near $H_{c2}(T)$ as long as the LLL approximation is correct. Taking into account only the leading terms in the derivative of the free-energy density the scaling function for the transport energy is obtained to

$$\frac{U_\phi(T,H)}{\sqrt{HT}}\frac{s(dH_{c2}/dT)}{A} = \sqrt{(At)^2+2} - At \ , \tag{11}$$

where s is the effective spacing of the Cu-O sheets and $t=[T-T_c(H)]/\sqrt{TH}$. The remarkable feature of the scaling function is the existence of a crossing temperature T^* at which all $U_\phi(T)$ curves for different H cross. The transport energy $U_\phi(T^*)$ at the crossing point is given by[78]

$$U_\phi(T^*) = \frac{k_B T^*}{s} \ . \tag{12}$$

The value of $U_\phi(T^*)$ only depends on the effective interlayer spacing which characterizes the 2D superconducting system.

Salamon and Shi[79] proposed a different scaling form based on a critical point analysis. For a 3D superconductor they obtained

$$U_\phi(T,H) = H^{1/2} G' \left[\frac{T-T_c}{T_c H^{3/4}} \right] , \tag{13}$$

where G' is the scaling function and T_c a field-independent mean-field transition temperature. The question, which scaling form is appropriate for which field regime is still a matter of controversy (see Refs. 77, 79, and 80). However, since for the 3D system the scaling variables $(T-T_c)/T_c H^{3/4}$ and $[T-T_{c2}(H)]/(TH)^{2/3}$ are not much different, there may be a crossover field range where the data can be described equally well by both schemes.

B. Seebeck effect

The Seebeck effect is associated with the generation of a longitudinal electric field E_x in the x direction due to a temperature gradient $\nabla_x T$ applied also in the x direction. In general the Seebeck coefficient is given by the ratio of the entropy flow density and the electrical current density, that is, the Seebeck coefficient S can be viewed as the transport entropy per unit charge. The Seebeck coefficient is defined as

$$S = \frac{E_x}{\nabla_x T} \ . \tag{14}$$

In the normal state the thermal diffusion current is compensated by the drift current due to a gradient $\nabla_x \mu$ in the electrochemical potential yielding

$$J_n \rho_n = -[S_n \nabla_x T + \nabla_x \mu / e] \ . \tag{15}$$

Here ρ_n and S_n are, respectively, the resistivity and the Seebeck coefficient in the normal state.

In the mixed state, in contrast to the Nernst effect, the Seebeck effect is dominated by the transport of quasiparticles. It has been shown experimentally that the thermal diffusion of quasiparticles in the presence of an applied temperature gradient results in a pronounced Seebeck effect.[29] As discussed by Ginzburg[30] for zero magnetic field and extended recently for the case of finite fields,[32] the appearance of a pronounced Seebeck effect in the mixed state can be understood in terms of a two-fluid counterflow picture. In the following we summarize this discussion.

It follows from the London equations that the microscopic electric field outside of a nonmoving vortex is zero. Then the continuity of the tangential component of the microscopic field at the vortex core boundary results in the condition

$$J_n \rho_n = -S_n \nabla_x T \ , \tag{16}$$

where J_n is the thermal diffusion current inside the vortex core. Charge conservation, in turn, requires the backflow of a supercurrent, $J_b = -J_n$, outside the core. As shown in Fig. 1(a) the backflow current has a dipolar form.[81,82] The backflow contribution to the superfluid velocity is added to the circular velocity of the vortex line itself on one side and subtracted from it on the other causing a force on the vortex line perpendicular to the applied temperature gradient. In the absence of pinning this force results in vortex motion perpendicular to the direction of the applied temperature gradient. For the moving vortices the counterflowing supercurrent density continues its flow as a normal current right through the

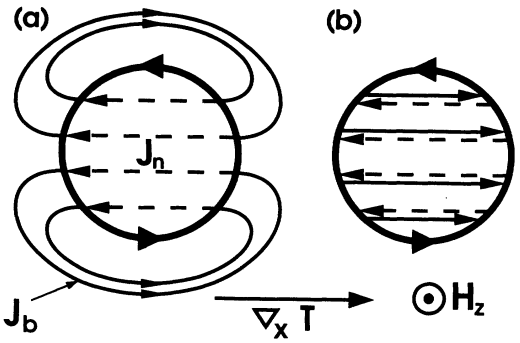

FIG. 1. Normal current density inside the vortex core (dashed lines) and dipolar counterflow pattern of the supercurrent density near the vortex core in the presence of a temperature gradient in horizontal direction for a pinned vortex (a). In (b) the situation for the moving vortex is shown.

vortex core, canceling the thermal diffusion current inside the core [see Fig. 1(b)]. Hence, according to Eqs. (14)–(16) and using $E_x = -\nabla_x \mu/e$ (the chemical part of μ is assumed constant), we obtain[29,32]

$$\frac{E_x(T)}{\nabla_x T} = S_F(T) = S_n(T)\frac{\rho_F(T)}{\rho_n(T)} . \tag{17}$$

Here S_F and ρ_F are the thermopower and the longitudinal resistivity in the flux motion state, respectively.

Anisotropy and fluctuation effects

We first discuss the case where the temperature gradient is applied parallel to the Cu-O sheets. According to Eq. (17) the normalized Seebeck electric field is determined by the resistivity and the Seebeck coefficient in the normal state and the flux motion resistivity in the mixed state. Let us compare these quantities for superconducting materials with similar Cu-O planes but different anisotropy such as $YBa_2Cu_3O_{7-\delta}$ and $Bi_2Sr_2CaCu_2O_{8+x}$. Both materials have Cu-O double layers. Therefore, if the doping of these layers is similar, in the normal state the resistivity and the Seebeck coefficient along the Cu-O sheets are expected to be about the same for both materials in agreement with experimental results. In contrast, the resistivity in the flux motion state is different for both materials, since the pinning of magnetic-flux lines in the mixed state and, hence, $\rho_F(T)$ strongly depends on the coupling between the Cu-O sheets, i.e., on the anisotropy. From this we conclude that the sign and the absolute magnitude of the normalized Seebeck electric field of cuprate superconductors with similar Cu-O sheets but different anisotropy is similar at the transition temperature, whereas the temperature dependence of $E_x/\nabla_x T$ in the mixed state may be quite different. We note, however, that the sign and absolute value of S_n sensitively depends on doping.[83–85]

For the temperature gradient applied perpendicular to the Cu-O sheets the situation is completely different. In this case the sample can be considered as a series connection of thermocouples which is formed by the layered high-T_c materials in a natural way. That is, the high-T_c materials can be viewed as a thermopile of atomic layers consisting of the Cu-O sheets and the charge reservoir layers separating them.[86] The presence of a temperature gradient perpendicular to the Cu-O sheets results in a temperature difference ΔT between the different Cu-O sheets. Due to the large number of stacked thermocouples a large thermoelectric voltage $V = N(S_A - S_B)\Delta T$ is obtained, where N is the number of elements and $S_A - S_B$ is the difference of the Seebeck coefficients of the two involved materials.

As discussed above fluctuation effects play an important role over an extended temperature range around T_c. Due to the presence of superconducting fluctuations the Seebeck voltage is reduced over a considerable temperature range above $T_{c2}(H)$. Measurements of the Seebeck effect at $T > T_c$ allow the study of these fluctuation effects. However, in contrast to the Nernst effect the measurement of the fluctuation contribution is difficult, since the large normal-state contribution has to be subtracted. Therefore, in our experiments fluctuation effects have been studied only for the Nernst effect.

C. Hall effect

In general, the Hall effect in the mixed state in most cases has been studied by electrical transport experiments employing the Lorentz force of an applied transport current density. There are two interesting features which have not yet been clarified in detail. First, the Hall coefficient changes sign over a range of magnetic fields just below the transition temperature.[34–42] The second feature is a striking scaling behavior of the form $\rho_{xy} \propto \rho_{xx}^{\beta}$, which has been observed for YBCO,[44,43] BSCCO,[46] and TBCCO.[42] Here, ρ_{xx} and ρ_{xy} are the longitudinal and Hall resistivities in the mixed state, respectively, and β typically ranges between 1.7 and 2.0. The sign anomaly has found various explanations such as effects of superconducting fluctuations,[47,48] phenomenological and microscopic modifications of the damping force,[23,49] or a theory that includes pinning in the standard Bardeen-Stephen theory[87] for flux motion.[50] The scaling relation between ρ_{xy} and ρ_{xx} has been discussed by Dorsey and Fisher in terms of a vortex-glass transition in a 3D vortex system with weak disorder.[51,52] Here, the scaling behavior was explained as a result of the glassy scaling near the vortex-glass transition. The Hall effect itself was attributed to a particle-hole asymmetry. In the vicinity of the vortex-glass transition this asymmetry is assumed to scale with a power of the vortex-glass correlation length.

More recently, Vinokur *et al.* explained the scaling behavior as a general feature of any vortex state with disorder dominated dynamics.[53] An exact value of 2 is predicted for the exponent β in the scaling relation. In the absence of pinning a scaling relation

$$\rho_{xy} = \rho_{xx}^2 \frac{\alpha}{H\Phi_0} = \rho_{xx}^2 \frac{\eta}{H\Phi_0}\tan\theta_H \tag{18}$$

immediately follows from the force balance equation

$$\Phi_0 \mathbf{J}\times\mathbf{n} - \alpha\mathbf{u}\times\mathbf{n} - \eta\mathbf{u} = 0 \tag{19}$$

using the relation $\mathbf{E}=-(\mathbf{u}\times\mathbf{H})$ and assuming that the Hall angle $\tan\theta_H=\alpha/\eta$ is small. Here, $\mathbf{J}$ is the transport current density, $\mathbf{u}$ is the vortex velocity, $\mathbf{n}$ the unit vector in the direction of the applied magnetic field, and the coefficient α determines the sign and magnitude of the Hall angle. In the presence of pinning the scaling relation is also obtained, since pinning only renormalizes the friction coefficient, whereas the Hall coefficient remains unchanged. As discussed in detail by Vinokur *et al.*[53] the random pinning potential is only determined by the relative positions of the vortices and the pins. Therefore, it is invariant under time reversal, that is, the averaged pinning force is invariant under reversal of the magnetic field. The average pinning force then is opposite to the vortex velocity $\mathbf{u}$ and can be expressed as $\langle F_{\rm pin}\rangle=-\gamma(u)\mathbf{u}$. The terms perpendicular to $\mathbf{u}$ cancel due to symmetry reasons. In Eq. (18) only the friction coefficient η then has to be replaced by $\eta^*=\eta+\gamma$. Note that the theories of Dorsey *et al.* and Vinokur *et al.* are of an entirely different nature. Critical phenomena, which are the basis of the Dorsey theory are not treated by the force balance approach of Vinokur *et al.* Interestingly, both theories predict a similar scaling behavior.

Information on the Hall coefficient also can be obtained by experiments employing the thermal force of an applied temperature gradient.[32,54] In the following we will take into account the Hall effect of both diffusing species, which has been neglected in Secs. II A and II B. In the presence of a temperature gradient the driving (Lorentz) force $\Phi_0\mathbf{J}\times\mathbf{n}$ in the force balance equation has to be replaced by the thermal force $\Phi_0\mathbf{J}_{\rm th}\times\mathbf{n}$ with[32]

$$\mathbf{J}_{\rm th}=\{(S_n\nabla_x T/\rho_n),\quad -S_\phi\nabla_x T/\Phi_0-(S_n\nabla_x T/\rho_n)\beta,\,0\}\ . \tag{20}$$

Using the relation $\mathbf{E}=-(\mathbf{u}\times\mathbf{H})$ the longitudinal and the transverse electric fields are obtained to

$$\frac{E_x}{\nabla_x T}=\frac{S_n}{\rho_n}\rho_{xx}(1+\tan\theta_H^2)+\frac{S_\phi}{\Phi_0}\rho_{xy}\ , \tag{21}$$

$$\frac{E_y}{\nabla_x T}=\frac{S_\phi}{\Phi_0}\rho_{xx}\ . \tag{22}$$

Deriving the expressions for the longitudinal and the transverse electric field we have assumed that the Hall coefficients for the diffusing vortices and quasiparticles are the same as expected according to the Bardeen-Stephen model.[87] Expressions similar to Eqs. (21) and (22) have been obtained recently by Samoilov, Yurgens, and Zavaritsky.[33] They also correspond to the result obtained by Maki[88] from the time-dependent Ginzburg-Landau theory.

It is evident from Eqs. (21) and (22) that information on the Hall effect in the mixed state can be obtained by measurements employing the thermal force of an applied temperature gradient. Equations (21) and (22) show that there should be no first-order Hall contribution to the transverse electric field $E_y/\nabla_x T$. In this context it is important to realize that the longitudinal electric field is generated by the thermal diffusion of quasiparticles in the normal core of the vortices parallel to the temperature gradient, which in turn results in the motion of the vortices perpendicular to $\nabla_x T$. It has been shown in detail recently[32] that the Hall effect of the diffusing quasiparticles and vortices cancel each other leaving only a second-order effect.

According to Eqs. (21) and (22) the Hall tangent $\tan\theta_H=\rho_{xy}/\rho_{xx}$ can be obtained by subtracting $(S_n/\rho_n)\rho_{xx}$ from the measured normalized longitudinal electric field and dividing the remaining quantity $\Delta S=(S_\phi/\Phi_0)\rho_{xy}$ by the measured transverse electric field. For the calculation of ΔS the measured $\rho_{xx}(T)$ dependence is used and $S_n(T)$ and $\rho_n(T)$ in the mixed state are obtained by linearly extrapolating the normal-state temperature dependence. The *thermal* Hall angle $\tan\theta_H^{\rm th}$ derived in this way was found to be much larger than that obtained from measurements employing the Lorentz force of an applied transport current density.[32]

A possible explanation of the much larger Hall angle in thermal force measurements is the presence of vortex-antivortex pairs. Due to their layered structure the high-temperature superconductors are highly anisotropic and 2D effects play a pronounced role in the mixed state of these materials. In particular, several experiments indicate the presence of a Kosterlitz-Thouless (KT) transition[89,90] at a temperature $T_{\rm KT}$ well below the mean-field transition temperature T_{c0}.[91,92] The KT transition is associated with the thermal creation of vortex-antivortex pairs in the absence of an external magnetic field. Below $T_{\rm KT}$, there are bound vortex-antivortex pairs, whereas above $T_{\rm KT}$ the pairs dissociate. The motion of the unbound pairs under the action of a driving force gives rise to finite dissipation. Note that there is an important difference between the Lorentz force and the thermal force. Whereas the Lorentz force depends on vorticity, the thermal force acts in the same direction for both vortices and antivortices. It has been shown recently[93] that in the presence of vortex-antivortex pairs the thermal Hall tangent can be expressed as

$$\tan\theta_H^{\rm th}=\left[\frac{N_B^+ +N_B^-}{N_B^+ -N_B^-}\right]\tan\theta_H\ . \tag{23}$$

In contrast, the Hall tangent $\tan\theta_H^L$ derived from Lorentz force measurements is given by

$$\tan\theta_H^L=\left[\frac{N_B^+ -N_B^-}{N_B^+ +N_B^-}\right]\tan\theta_H\ . \tag{24}$$

Here, N_B^+ and N_B^- are the total number of free vortices and antivortices at a finite applied magnetic field, respectively. Applying an external magnetic field increases the number of free vortices and antivortices by reducing the effective KT transition temperature and introduces a fixed difference $N_B^+ -N_B^- =B/\Phi_0$. Equations (23) and (24) show that the Hall angle derived from thermal force and Lorentz force measurements are, respectively, enhanced and reduced by a factor $C=(N_B^+ +N_B^-)/(N_B^+ -N_B^-)$. This is in agreement with recent Lorentz force measurements on multilayer thin films[94] and thermal force measurements on $YBa_2Cu_3O_{7-\delta}$ films.[32,93] Note that the number of free vortices and antivortices can be

quite large resulting in $C \gg 1$ even at high magnetic fields.

We finally have to discuss the effect of pinning on the validity of Eqs. (21) and (22), which have been derived without taking into account the effect of pinning. Using the arguments of Vinokur *et al.*[53] it can be shown that the longitudinal and transverse electric field normalized to the longitudinal resistivity do not depend on the pinning strength.[45] That is, in the pinned regime both the Nernst and the Seebeck coefficients are proportional to the longitudinal resistivity independent of the pinning strength and Eqs. (21) and (22) also hold in the presence of pinning.

Anisotropy and fluctuation effects

In the following we will restrict our discussion to the case where the temperature gradient (or transport current) is applied parallel to and the magnetic field perpendicular to the Cu-O sheets. Materials with different degrees of anisotropy are expected to have different pinning strength for flux lines in the mixed state. According to the theoretical treatment of Vinokur *et al.*,[53] the scaling behavior of the Hall resistivity is a universal feature of the mixed state independent of the detailed pinning strength. In contrast, the sign anomaly of the Hall effect has been explained by Wang and Ting[50] in terms of a pinning induced backflow in the vortex core. That is, according to this model the sign anomaly should strongly depend on the pinning strength and, hence, the anisotropy of the material. Using materials with different anisotropy such as $YBa_2Cu_3O_{7-\delta}$ and $Bi_2Sr_2CaCu_2O_{8+x}$ the effect of different pinning strengths on the Hall effect in the mixed state can be studied experimentally.

Data on the Hall effect in the fluctuation regime are scarce.[23,95] A general problem in evaluating Hall effect data in the fluctuation regime is the difficulty to separate the fluctuation contribution to the Hall resistivity, since the Hall effect is strongly temperature dependent in the normal state. Information on the fluctuation contribution to the Hall resistivity would be highly important. Recently, in some models the sign anomaly of the Hall effect was attributed to the negative value of the particle-hole asymmetry parameter and fluctuation effects (Refs. 47, 48, 51, 96, and 97).

III. EXPERIMENTAL TECHNIQUES

A. Sample preparation

For our experiments we used epitaxial, *c*-axis-oriented $YBa_2Cu_3O_{7-\delta}$ and $Bi_2Sr_2CaCu_2O_{8+x}$ films grown on (100) $SrTiO_3$ substrates. The $YBa_2Cu_3O_{7-\delta}$ films were prepared by hollow cathode magnetron sputtering from a stoichiometric YBCO target. The films were deposited at a substrate temperature of about 780 °C in a 60 Pa Ar/O_2 (1.5/1.0) atmosphere. The deposition rate was about 20 Å/min. At the end of the deposition process the films were cooled slowly in 80-kPa oxygen with a dwell time of 10 min at $T=450$ °C. The $YBa_2Cu_3O_{7-\delta}$ films prepared in this way are perfectly *c*-axis oriented and have zero resistance critical temperatures above 90 K and critical current densities of about 5×10^6 A/cm^2 at 77 K. Typically, the normal-state resistivity of the films at $T=100$ K was 100 $\mu\Omega$ cm. The thickness of the films used in our experiments was 200 nm. The $Bi_2Sr_2CaCu_2O_{8+x}$ films were prepared by dc sputtering from a single planar target of 2:2:1:2 composition.[98,99] As sputtering parameters we used a discharge current of 400 mA and an applied voltage of 310 V in an oxygen atmosphere of 3.0 hPa. The growth rate was about 30 Å/min. The temperature at the substrate surface was 830 °C as measured by a thermoelement. After the deposition the films were annealed at the deposition temperature and oxygen atmosphere for 45 min in order to increase the critical temperature to values well above 80 K. The $Bi_2Sr_2CaCu_2O_{8+x}$ films prepared in this way are *c*-axis oriented and have a smooth surface. The film thickness was about 400 nm. The films had a zero resistance critical temperature of typically above 85 K, a critical current density well above 10^5 A/cm^2 at 77 K, and a normal-state resistivity of about 100 $\mu\Omega$ cm at $T=100$ K.

For our experiments the thin films were patterned into two parallel strips A and B and a strip C perpendicular to strips A and B as shown in Fig. 2. The strips were 100 μm wide and about 6 mm long. Strip A and B are perpendicular to the applied temperature gradient and are used for measuring the Nernst effect, while strip C, which is parallel to the applied temperature gradient, is used for measuring the Seebeck effect. Without applied temperature gradient the sample configuration shown in Fig. 2, which represents a Hall bar geometry, can be used for measuring the Hall effect. The patterning of both the $YBa_2Cu_3O_{7-\delta}$ and the $Bi_2Sr_2CaCu_2O_{8+x}$ films was performed by standard photolithography and Ar ion-beam etching.[100] During the ion-beam etching the samples were cooled to liquid-nitrogen temperature in order to avoid any oxygen loss during the etching process. The contact pads were covered by a 50-nm Ag film prior to

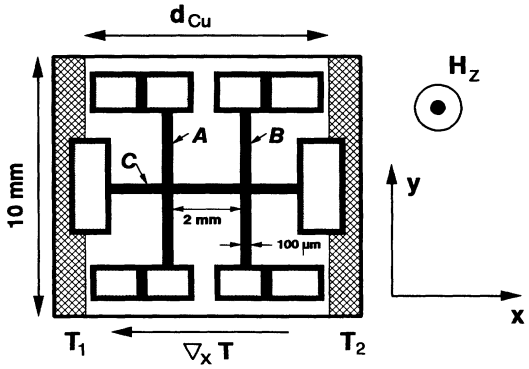

FIG. 2. Sketch of the thin-film sample configuration used in our experiments. The Nernst effect is measured either with strip A or B, whereas the Seebeck effect is measured with strip C. The hatched area indicates the substrate part that are glued onto the copper blocks which are kept at different temperatures in order to establish a temperature gradient along the *x* direction.

the etching process in order to obtain small contact resistance.

B. Measuring technique

In order to establish a temperature gradient across the thin film samples we have developed a sample holder, where the substrate is mounted on two gold-plated copper blocks. The copper blocks are thermally decoupled and their temperature can be controlled separately with an accuracy of better than 5 mK. Details on the sample holder are reported in Ref. 18. Setting the temperature of the copper blocks to different values T_1 and T_2, a temperature gradient is established.

A basic problem is the unknown thermal boundary resistance between the copper blocks and the substrate. Due to the finite boundary resistance the temperature gradient established along the substrate is always smaller than $(T_2-T_1)/d_{\mathrm{Cu}}$, where d_{Cu} is the distance between the copper blocks. In order to determine the exact value of the temperature gradient, the sample configuration of Fig. 2 can act itself as the thermometer. First, the temperature dependent resistivity of strips A and B, $\rho_{\mathrm{A}}(T)$ and $\rho_{\mathrm{B}}(T)$, are measured without any applied temperature gradient. Then the temperature of the copper blocks is set to different temperatures T_1 and T_2. Using the calibration curves $\rho_{\mathrm{A}}(T)$ and $\rho_{\mathrm{B}}(T)$ the temperature T_{A} and T_{B} of strip A and B, respectively, and the actual temperature gradient along the substrate, $(T_{\mathrm{B}}-T_{\mathrm{A}})/d$, can be determined precisely at the given temperature difference T_2-T_1 between the copper blocks. Here, d is the distance between strip A and B. As described in detail in Ref. 21, the sample configuration shown in Fig. 2 allows the precise control of the mean temperature of the strips and the applied temperature gradient. Typically, the mean temperature of strip A can be kept constant within less than 30 mK during the variation of the temperature gradient from -10 to $+10$ K/cm. Furthermore, the mean temperature of the strip can be varied in a controlled way at a fixed temperature gradient. For an applied temperature gradient of 1 K/cm the temperature difference between both edges of the 100-μm-wide strips used for taking the Nernst data is only 10 mK.

In our experiments the transverse Nernst electric field always is measured for the two opposite directions of the applied magnetic field in order to eliminate any unwanted contributions. The normalized Nernst electric field is determined by the antisymmetric part of the measured signals:

$$\frac{E_y}{\nabla_x T}=\frac{1}{2\nabla_x T}[E_y(+H)-E_y(-H)] .$$

The normalized Seebeck electric field

$$\frac{E_x}{\nabla_x T}=S_{\mathrm{TC}}=S_{\mathrm{Cu}}-S_{\mathrm{Sup}}$$

is given by the thermopower S_{TC} of the Cu/superconductor thermocouple. That is, the thermopower S_{Cu}, which is well known for high-purity copper, has to be subtracted to get S_{Sup}. Furthermore, since the magnetic-field dependence of S_{Cu} is weak in the investigated temperature range, one has

$$S_{\mathrm{TC}}(T,H)-S_{\mathrm{TC}}(T,0)\simeq S_{\mathrm{Sup}}(T,0)-S_{\mathrm{Sup}}(T,H) .$$

That is, plotting this quantity the effect of copper can be eliminated.

The resistive transition and the Hall effect are measured using a standard four-probe and Hall bar geometry. In our experiments the Hall resistivity is obtained from the antisymmetric part of the transverse electric field changing the direction of both the applied transport current and magnetic field as

$$\rho_{xy}=\frac{1}{4J}\{[E_y(+H,+J)-E_y(+H,-J)] -[E_y(-H,+J)-E_y(-H,-J)]\} .$$

The applied transport current density typically was about 10 A/cm^2 for the resistive transition and about 1000 A/cm^2 for the Hall measurements.

IV. EXPERIMENTAL RESULTS AND DISCUSSION

A. Nernst effect

Figure 3 shows the temperature dependence of the resistivity ρ and the normalized Nernst electric field

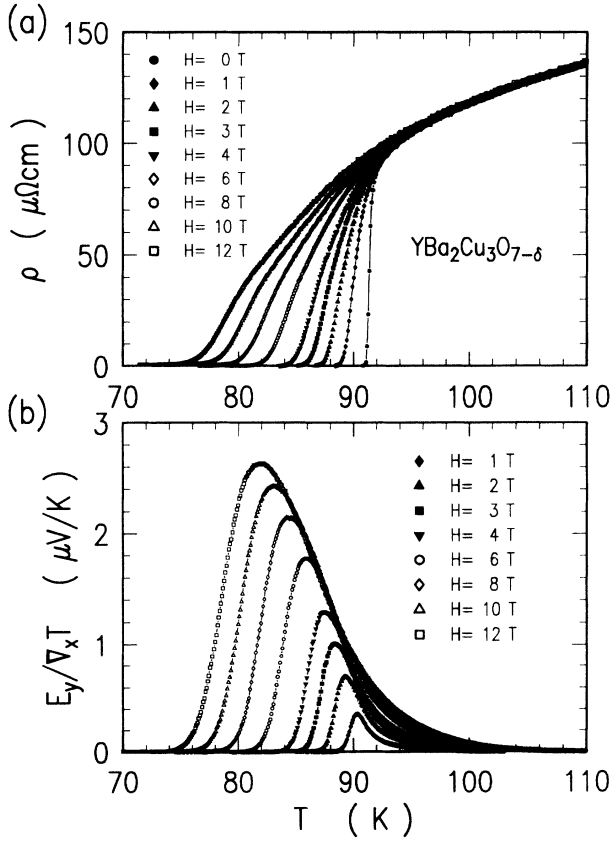

FIG. 3. Resistivity ρ (a) and normalized Nernst electric field $E_y/\nabla_x T$ (b) versus temperature for an epitaxial, c-axis-oriented $YBa_2Cu_3O_{7-\delta}$ film at different magnetic fields applied parallel to the c axis of the film.

$E_y/\nabla_x T$ of an epitaxial $YBa_2Cu_3O_{7-\delta}$ film for different magnetic fields $\mathbf{B}\|c$ up to 12 T. In the presence of the applied field the usual broadening of the resistive transition is observed. The Nernst electric field was measured for opposite magnetic-field direction in the stationary state at an applied temperature gradient of 1 K/cm using a Keithley nanovolt meter. The voltage resolution in our experiment was better than about 5 nV corresponding to an electric-field resolution of less than 10 nV/cm for our sample configuration. At the low-temperature side the Nernst electric field becomes unmeasurably small at the same temperature as the resistivity because of the increasing flux-pinning strength. In the high-temperature regime above the thermodynamic critical temperature T_c a considerable Nernst electric field is detected because of fluctuation effects. For the different high quality epitaxial $YBa_2Cu_3O_{7-\delta}$ films the measured temperature dependences of the resistivity and the normalized Nernst electric field are very similar. Deviations are observed for films containing a large number of grain boundaries as discussed in detail in Ref. 21.

Figure 4 shows the temperature dependence of the resistivity and the normalized Nernst electric field $E_y/\nabla_x T$ of an epitaxial $Bi_2Sr_2CaCu_2O_{8+x}$ film for magnetic fields $\mathbf{B}\|c$ up to 12 T. Figure 4 clearly shows that for $Bi_2Sr_2CaCu_2O_{8+x}$ the broadening of the resistive transition is much stronger than for the $YBa_2Cu_3O_{7-\delta}$ film because of the different flux-pinning behavior of $Bi_2Sr_2CaCu_2O_{8+x}$. Again the Nernst electric field was measured in the stationary state at an applied temperature gradient of 1 K/cm. Figure 4 shows that going to low temperatures the Nernst electric field becomes unmeasurably small at the same temperature as the resistivity as observed for the $YBa_2Cu_3O_{7-\delta}$ films. Due to the larger anisotropy of $Bi_2Sr_2CaCu_2O_{8+x}$ and the related weaker flux-pinning strength the temperature regime, where a finite Nernst electric field is observed, is much wider than for $YBa_2Cu_3O_{7-\delta}$. Also, the temperature regime in which fluctuation effects play a dominant role is much wider for $Bi_2Sr_2CaCu_2O_{8+x}$ than for $YBa_2Cu_3O_{7-\delta}$. A significant Nernst electric field is observed up to temperatures well above the thermodynamic critical temperature T_c due to fluctuation effects. As discussed above, the wider fluctuation regime of $Bi_2Sr_2CaCu_2O_{8+x}$ is expected because of the larger anisotropy of this material as compared to $YBa_2Cu_3O_{7-\delta}$. We investigated several $Bi_2Sr_2CaCu_2O_{8+x}$ thin film samples. For high-quality epitaxial films the measured $\rho(T)$ and $E_y(T)/\nabla_x T$ dependences are, respectively, very similar.

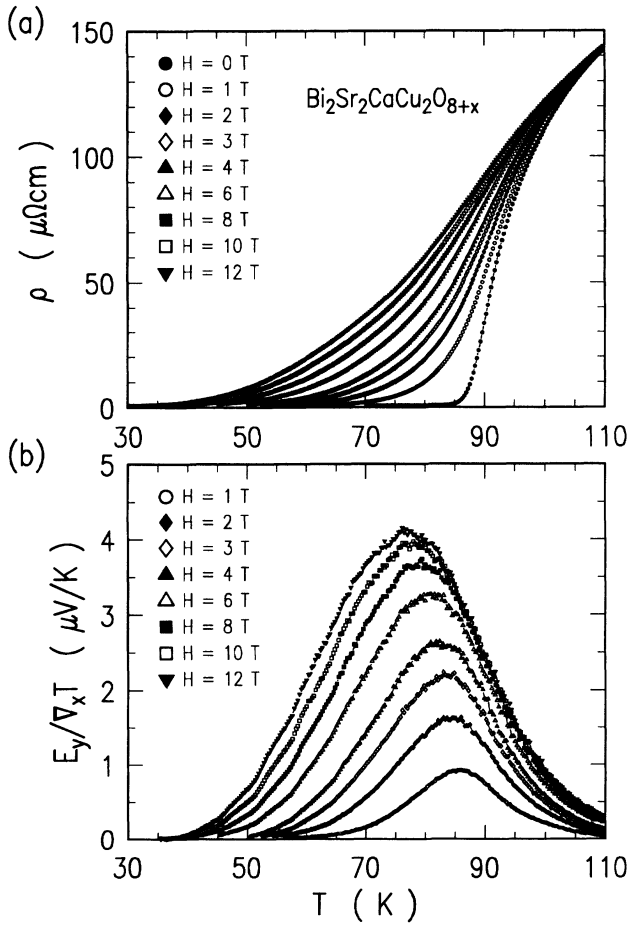

FIG. 4. Resistivity ρ (a) and normalized Nernst electric field $E_y/\nabla_x T$ (b) versus temperature for an epitaxial, c-axis-oriented $Bi_2Sr_2CaCu_2O_{8+x}$ film at different magnetic fields applied parallel to the c axis of the film.

1. Transport energy and upper critical field

From the data for $YBa_2Cu_3O_{7-\delta}$ shown in Fig. 3 we have derived the transport energy per unit length of flux line, $U_\phi = TS_\phi$, according to Eq. (3). The result is shown in Fig. 5(a) where we have plotted U_ϕ versus T for different values of the applied magnetic field. Going from low to high temperatures, U_ϕ initially decreases about linearly with increasing temperature and then shows a fluctuation induced tail extending well above T_c. From the linear part of the $U_\phi(T)$ curves we can derive the slope dU_ϕ/dT, which is plotted in Fig. 5(b) versus the applied magnetic field. We note that dU_ϕ/dT at fixed field is the more useful quantity for comparing the results of different experiments, since small variations in T_c affect this quantity much less than U_ϕ itself. For $B=4$ T we obtain $dU_\phi/dT = -2.5\times10^{-13}$ J/Km. This value is in good agreement with values obtained from measurements of the Nernst[23] and Ettingshausen effects[26] and the magnetization,[60] which range between about -2 and -6×10^{-13} J/Km.[21]

At $T=87$ K and $B=4$ T we measure a transport energy of 7×10^{-13} J/m corresponding to a transport entropy $S_\phi = 8\times10^{-15}$ J/Km. With the temperature gradient of 1 K/cm used in our experiment the thermal force per unit length acting on the flux lines is estimated to 8×10^{-13} J/m^2. The current density causing a Lorentz force of equal strength is only about 4×10^{-2} A/cm^2. In contrast, the current density used for measuring the resistivity [Fig. 3(a)] was about 1 A/cm^2. Therefore, it is important to clarify whether the different magnitude of the thermal force and the Lorentz force used for the measurement of ρ and $E_y/\nabla_x T$, respectively, affects the result derived for

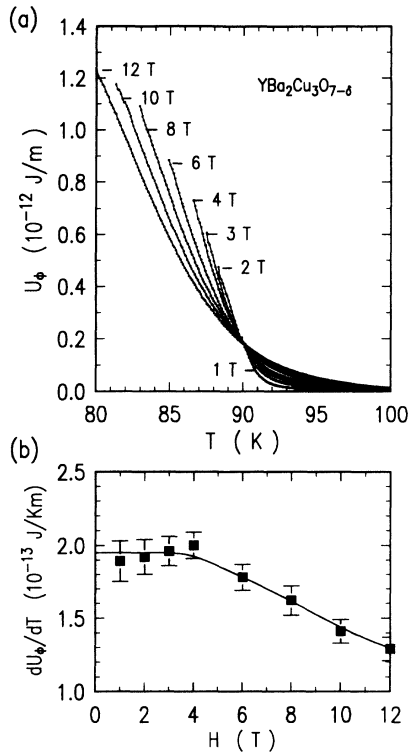

FIG. 5. Transport energy U_ϕ versus temperature for an epitaxial, c-axis-oriented $YBa_2Cu_3O_{7-\delta}$ film at different magnetic fields applied parallel to the c axis of the film. In (b) the slope $-dU_\phi/dT$ of the linear part of the $U_\phi(T)$ curves is plotted versus the applied magnetic field. The line is only for guiding the eye.

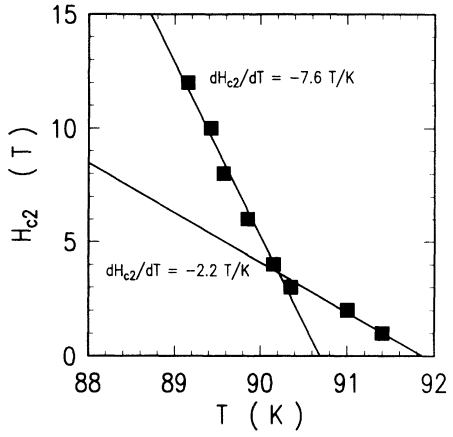

FIG. 6. Upper critical field H_{c2} plotted versus temperature for an epitaxial, c-axis-oriented $YBa_2Cu_3O_{7-\delta}$ film. The lines are linear fits to the data points for $T>90$ K and $T<90$ K, respectively.

the transport energy. This would be expected if the $E_y(J_y)$ and the $E_y(\nabla_x T)$ dependences are nonlinear. Our measurements showed that both dependences are linear in the J_y and $\nabla_x T$ regime of our experiments in agreement with the expected thermally activated nature of flux motion in our sample.[16]

According to Eq. (6) we can derive $T_{c2}(H)$ and, hence, $H_{c2}(T)$ by linearly extrapolating the linear part of the $U_\phi(T)$ dependences to zero. The H_{c2} values obtained for $YBa_2Cu_3O_{7-\delta}$ in this way are plotted versus temperature in Fig. 6. According to Fig. 6 the upper critical field slope is not constant. Whereas for lower fields we obtain $dH_{c2}/dT=-2.2\pm0.3$ T/K, for higher fields we have $dH_{c2}/dT=-7.6\pm0.5$ T/K. In our calculation the temperature dependence of the function $L_D(T)$ was neglected. The $H_{c2}(T)$ dependence shown in Fig. 6 is very similar to that obtained by Palstra *et al.*[26] and contradicts the GL result predicting a constant upper critical field slope near T_c. This discrepancy is likely caused by the fact that the high-field GL result [Eq. (6)] is not applicable for evaluating part of the data. Figure 5(b) clearly shows that the slope dU_ϕ/dT decreases significantly with increasing magnetic field starting from about $B=4$ T. This appears to be an artefact of our evaluation of the experimental data.

For the higher fields the slope dU_ϕ/dT is evaluated at lower temperatures. However, this regime of the H-T phase space no longer belongs to the high-field regime due to the large upper critical field slope. For example, with the zero-field critical temperature of 92 K and $dH_{c2}/dT=-2.2$ T/K we estimate an upper critical field $H_{c2}\simeq22$ T at $T=82$ K. Hence, an applied field of 12 T only corresponds to an intermediate field at this temperature and the high-field GL result cannot be applied to derive $H_{c2}(T)$. Therefore, it is likely that the increase of dH_{c2}/dT from about -2 to -7 T/K is caused by an improper evaluation of the experimental data. As shown below a scaling plot of $U_\phi(T)$ in the fluctuation regime also yields $dH_{c2}/dT=-2$ T/K.

For $Bi_2Sr_2CaCu_2O_{8+x}$ we have used the experimental data of Fig. 4 to derive $U_\phi(T)$. The result is shown in Fig. 7 for different values of the applied magnetic field. In contrast to the $YBa_2Cu_3O_{7-\delta}$ data a linear part in the $U_\phi(T)$ dependences can be observed only for the lowest field values. At temperatures close to T_c pronounced fluctuation effects prevent us from observing the linear $U_\phi(T)$ dependence, whereas at lower temperatures we are already far from the GL high-field limit. Hence, it is impossible to determine $H_{c2}(T)$ by linearly extrapolating the $U_\phi(T)$ dependences. As will be shown below, $H_{c2}(T)$ can be obtained by a scaling plot according to Eq. (10). Evaluating dU_ϕ/dT for $B=1$ T we obtain $dU_\phi/dT=-5\times10^{-14}$ J/Km. This value is about 3.5 times smaller than that obtained for $YBa_2Cu_3O_{7-\delta}$. However, for $B=1$ T the slope dU_ϕ/dT is evaluated in the temperature regime between about 65 and 75 K. In this temperature regime the upper critical field is larger than about 20 T, that is, our applied field is much too small for probing the high-field regime. Therefore, one expects the slope derived using the GL high-field approximation to be too small. Taking this into account we conclude that dU_ϕ/dT is about the same for $Bi_2Sr_2CaCu_2O_{8+x}$ and $YBa_2Cu_3O_{7-\delta}$ as expected from our theoretical considerations. Comparing the absolute value of the transport entropy at $B=4$ T and $T=0.95T_c$

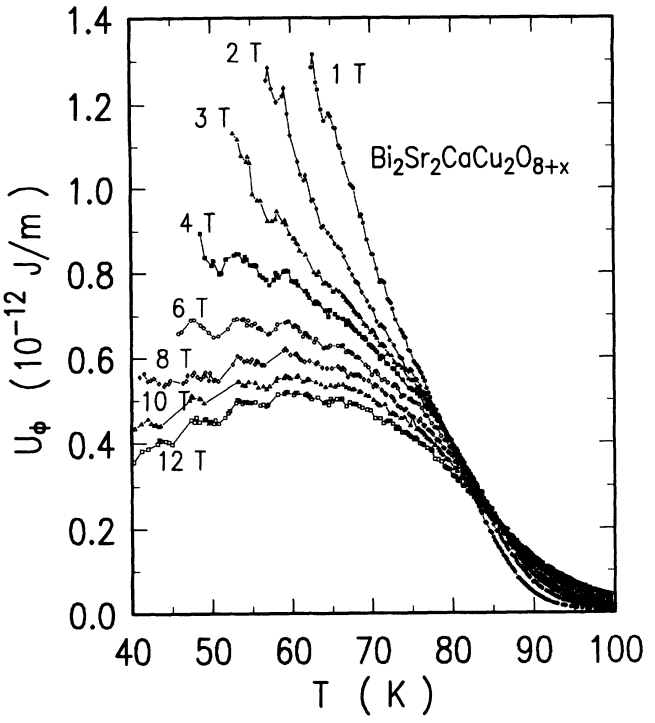

FIG. 7. Transport energy U_ϕ versus temperature for an epitaxial, c-axis-oriented $Bi_2Sr_2CaCu_2O_{8+x}$ film at different magnetic fields applied parallel to the c axis of the film.

we obtain $S_\phi = 6.5\times10^{-13}$ and 3.7×10^{-13} J/Km for $YBa_2Cu_3O_{7-\delta}$ and $Bi_2Sr_2CaCu_2O_{8+x}$, respectively. Figure 7 also indicates that $U_\phi(T)$ has a maximum between about 50 and 60 K. This is expected since $S_\phi = U_\phi/T \to 0$ for $T \to 0$.

Recently, $dU_\phi/dT = -4.5\times10^{-15}$ J/Km and -3.2×10^{-15} J/Km has been measured for single- and polycrystalline $Bi_2Sr_2CaCu_2O_{8+x}$ samples, respectively.[25,28] These values are by a factor of about 10 smaller than those obtained for our epitaxial thin film samples. The reason for that may be the different sample quality used in the different experiments. It was shown recently for $YBa_2Cu_3O_{7-\delta}$ (Ref. 21) that the derived value of dU_ϕ/dT is strongly reduced by the presence of grain boundaries in the sample. This especially may explain the small value of dU_ϕ/dT obtained for the polycrystalline BSCCO sample.

As pointed out above a significant part of the experimental data belongs to the intermediate- or low-field regime and cannot be evaluated using the high-field approximation. In Fig. 5(a), the failing of the high-field GL approximation manifests itself in a notable field dependence of the slope dU_ϕ/dT at constant temperature. In order to analyze our data in the intermediate-field regime we have fitted our data to the theory of Hao and coworkers.[60,61] For fitting the data usually the Ginzburg-Landau parameter κ is used as the fitting parameter. However, the value of κ obtained from the fitting procedure strongly increases with temperature for $T > 87$ K. This behavior has been observed also by other authors[74,101] and may be attributed to fluctuation contributions which are not included in the Hao-Clem theory. Therefore, we used a constant value for κ for the whole temperature regime we have studied.

In Fig. 8(a) we have plotted the magnetization versus the applied magnetic field in reduced units. Both quantities have been normalized by $\sqrt{2}H_c(T)$, where $H_c(T)$ is the thermodynamic critical magnetic field. The magnetization has been obtained from the transport energy according to Eqs. (5) and (6). The line in Fig. 8(a) shows a fit of the experimental data to the BCS temperature dependence.[102] The best fit is obtained for $\kappa = 75$. The data points used for the fitting process were in the range $82.9 \le T \le 88.3$ K and $1 \le H \le 12$ T. In Fig. 8(b) the H_c versus T dependence determined by the fitting process is shown. The line again shows the BCS result. The fit to the BCS result yields $H_c(T=0) = 1.24$ T and $T_c(H=0) = 93.9$ K. Using the relations $\sqrt{2}H_c = \kappa\Phi_0/(2\pi\lambda_{ab}^2)$ and $H_{c2}(T) = \sqrt{2}\kappa H_c(T)$ we obtain $\lambda_{ab}(0) = 1170$ Å and $dH_{c2}/dT = -2.3$ T/K at T_c.

For $Bi_2Sr_2CaCu_2O_{8+x}$ it is very difficult to obtain a reasonable fit of the measured transport energy data to the Hao-Clem theory. Fitting the data a strongly temperature dependent GL parameter is obtained. As already mentioned above, this is most likely caused by fluctuation contributions. For the very anisotropic $Bi_2Sr_2CaCu_2O_{8+x}$ fluctuation effects are relevant over a much wider temperature regime than for $YBa_2Cu_3O_{7-\delta}$.

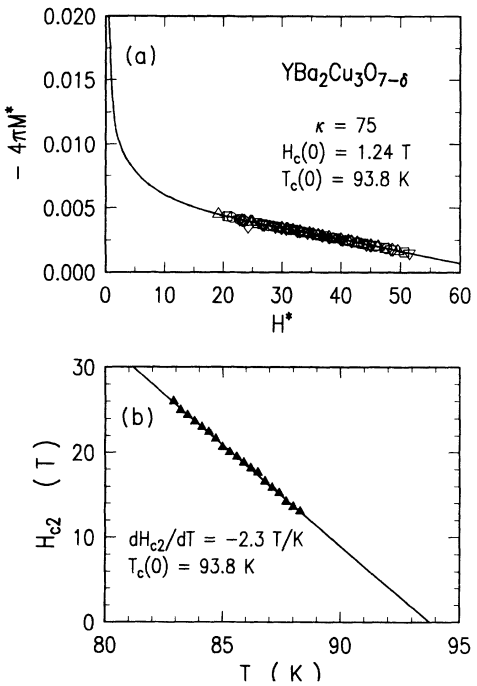

FIG. 8. (a) Magnetization versus applied field in reduced units. The symbols represent the same data as in Fig. 5(a). The scaling factor $\sqrt{2}H_c(T)$ and the GL parameter κ are obtained as described in the text and in Ref. 60. The line shows the BCS temperature dependence of H_c. (b) Temperature dependence of H_{c2} (symbols) deduced from the magnetization data and fit to the BCS temperature dependence (solid curve).

This prevents the use of the Hao-Clem theory, which does not take into account fluctuation contributions. As shown below, for $Bi_2Sr_2CaCu_2O_{8+x}$ reliable values for the upper critical field slope and the coherence length can be obtained from a scaling plot of the transport energy in the fluctuation regime.

2. *Fluctuation effects*

Figures 3 and 4 show that the normalized Nernst electric field $E_y/\nabla_x T$ does not disappear for $T > T_c$ for both $YBa_2Cu_3O_{7-\delta}$ and $Bi_2Sr_2CaCu_2O_{8+x}$. The tail of the $E_y/\nabla_x T$ or U_ϕ versus T curves apparently is caused by fluctuation effects with the contribution of fluctuations increasing with increasing magnetic field. Since in the normal state the Nernst electric field is negligibly small the fluctuation contribution can be measured easily. In Fig. 9 we have plotted the measured transport energy normalized to $(TH)^m$ versus $(T-T_{c2})$ also normalized to $(TH)^m$ for both $YBa_2Cu_3O_{7-\delta}$ [Fig. 9(a)] and $Bi_2Sr_2CaCu_2O_{8+x}$ [Fig. 9(b)]. The only fitting parameters in these scaling plots are the function $T_{c2}(H)$ and the exponent m. For the $YBa_2Cu_3O_{7-\delta}$ data a reasonable fit could be obtained only for $m=\frac{2}{3}$, whereas the

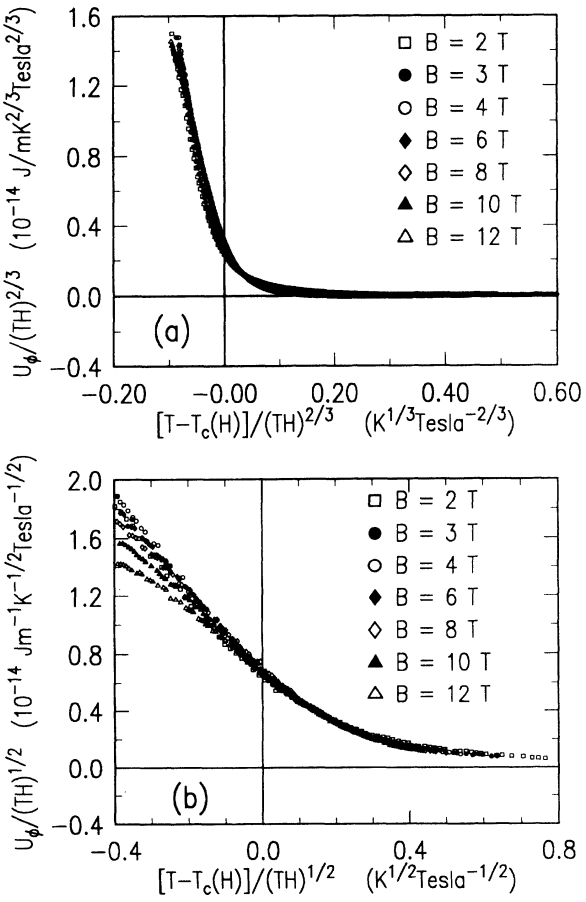

FIG. 9. Scaling plot of the transport energy of magnetic-flux lines obtained from an epitaxial, c-axis-oriented (a) $YBa_2Cu_3O_{7-\delta}$ and (b) $Bi_2Sr_2CaCu_2O_{8+x}$ thin film.

$Bi_2Sr_2CaCu_2O_{8+x}$ data could be fitted only for $m=\frac{1}{2}$. This is in agreement with the expected quasi-3D and quasi-2D behavior of $YBa_2Cu_3O_{7-\delta}$ and $Bi_2Sr_2CaCu_2O_{8+x}$, respectively. For both materials the best fit is obtained with a linear $T_{c2}(H)$ dependence close to the transition temperature. For $YBa_2Cu_3O_{7-\delta}$ and $Bi_2Sr_2CaCu_2O_{8+x}$ we obtained $T_{c2}(0)=92.4$ and 90.4 K and $dH_{c2}/dT=-2.4$ and -2.5 T/K, respectively.

For $YBa_2Cu_3O_{7-\delta}$ the value of dH_{c2}/dT agrees very well with that derived from the linear extrapolation of $U_\phi(T)$ in the high-field regime (see Fig. 6) and the fit to the Hao-Clem theory. This gives further evidence that the large value of dH_{c2}/dT of about -7 T/K is just caused by applying the high-field limit approximation [Eq. (6)] to the intermediate field regime. Furthermore, we note that the scaling behavior shown in Fig. 9(a) agrees well with the recent scaling analysis performed by Welp *et al.*[73] on the Ettingshausen effect data measured by Palstra *et al.*[26] Whereas the scaling analysis yields $dH_{c2}/dT=-1.9$ T/K, the linear extrapolation of the Ettingshausen coefficient applying the high-field limit yields -7 T/K similar to our result. For $Bi_2Sr_2CaCu_2O_{8+x}$ the derived values of $T_{c2}(0)=90.4$ K and $dH_{c2}/dT=-2.5$ T/K agree well with those obtained from magnetization measurements.[75]

The scaling form of Eq. (10) only applies to the high-field limit, since only the lowest Landau level was taken into account. Our data indicate that the actual range of applicability of this scaling form apparently is much wider than expected, in agreement with the scaling analysis of the Ettingshausen[73,77] and magnetization data.[75] Significant deviations from the scaling form are only found for $Bi_2Sr_2CaCu_2O_{8+x}$ at large negative values of $[T-T_{c2}(H)]/(TH)^{1/2}$. For $Bi_2Sr_2CaCu_2O_{8+x}$ the scaling function was found to agree well with the function derived by Tesanovic *et al.*[78] for a 2D superconducting system [Eq. (11)]. A similar result has been found by Li *et al.*[75] from magnetization measurements on $Bi_2Sr_2CaCu_2O_{8+x}$ single crystals.

Figure 7 shows the $U_\phi(T)$ curves have a crossing temperature T^* as predicted by the theory of Tesanovic *et al.*[78] It was observed that the crossing point is sharp only for applied fields smaller than about 5 T. For higher fields the crossing point is smeared out as shown by Fig. 7. For $H<5$ T we obtain $T^*=79.8$ K and $U_\phi^*(T^*)=4.1\times10^{-13}$ J/m. According to Eq. (12) these values result in an effective spacing between the superconducting layers of $s=26.2$ Å. This value is almost twice the value of 15.39 Å (half the unit-cell length along the c direction) expected for the Bi(2:2:1:2) system. Interestingly, a sharp crossing point also is observed for the $YBa_2Cu_3O_{7-\delta}$ sample [see Fig. 5(a)], which shows 3D scaling behavior.

3. *Material parameters*

Based on our experimental data we can derive several important material parameters of $YBa_2Cu_3O_{7-\delta}$ and $Bi_2Sr_2CaCu_2O_{8+x}$. The measured quantities and the deduced parameters are summarized in Table I. The values

TABLE I. Comparison of relevant material parameters of $YBa_2Cu_3O_{7-\delta}$ and $Bi_2Sr_2CaCu_2O_{8+x}$. The slope $-dU_\phi/dT$, the transport entropy per unit length of flux line S_ϕ, the upper critical field slope dH_{c2}/dT, and the zero-field critical temperature $T_{c2}(H=0)$ are directly obtained from our experimental data. The upper critical field $H_{c2}(T=0)$, the *ab*-plane coherence length ξ_{ab}, the GL parameter κ, and the screening length for currents in the *ab* plane λ_{ab} are deduced from the measured quantities as described in the text.

	$YBa_2Cu_3O_{7-\delta}$	$Bi_2Sr_2CaCu_2O_{8+x}$
$-dU_\phi/dT$ (J/Km)	2.5×10^{-13}	$>0.5\times10^{-13}$
$S_\phi(1T,0.95T_c)$ (J/Km)	6.5×10^{-15}	3.7×10^{-15}
$-dH_{c2}/dT$ (T/K)	2.4±0.2	2.5±0.2
$T_{c2}(H=0)$ (K)	93.0	90.4
$H_{c2}(T=0)$ (T)	150±20	158±13
ξ_{ab} (Å)	14.5±1.2	14.2±0.6
κ	75±5	<185±11
λ_{ab} (Å)	1170±100	<2630±160

of $H_{c2}(0)$ were derived using the Werthamer, Helfand, and Hohenberg theory.[103] The *ab*-plane coherence length is obtained from the upper critical field as $\xi_{ab}=(\Phi_0/2\pi H_{c2})^{1/2}$. Since in our experiments both dU_ϕ/dT and dH_{c2}/dT are measured, the GL parameter κ can be derived as

$$\kappa=\sqrt{(\Phi_0/9.28\pi)[(dH_{c2}/dT)/(dU_\phi/dT)]}\ . \qquad (25)$$

Equation (25) immediately follows from Eq. (6) for $\kappa\gg1$. For $YBa_2Cu_3O_{7-\delta}$ the value of $\kappa\simeq80$ derived according to Eq. (25) agrees well with that obtained from the fit to the Hao-Clem theory. We note that for $Bi_2Sr_2CaCu_2O_{8+x}$ the values derived for κ and λ_{ab} are slightly too large, since the value of dU_ϕ/dT is underestimated as discussed above. The parameters listed in Table I agree well with the values derived from other types of experiments (Refs. 26, 60, 73, 75, 101, and 104).

The material parameters listed in Table I are derived for magnetic fields applied perpendicular to the Cu-O sheets. That is, they are determined by the superconducting properties parallel to these layers. Table I clearly shows that the characteristic *ab*-plane material parameters of $YBa_2Cu_3O_{7-\delta}$ and $Bi_2Sr_2CaCu_2O_{8+x}$ are very similar. That is expected, since both materials have similar Cu-O double layers. The different anisotropy of both materials only influences the characteristic parameters in the *c* direction. The *c*-axis parameters are difficult to derive with *c*-axis-oriented thin-film samples. As will be shown elsewhere,[105] the *c*-axis coherence length and critical field can be obtained from magnetoresistance measurements in the fluctuation regime.

B. Seebeck effect

The sample configuration for measuring the Seebeck effect of $YBa_2Cu_3O_{7-\delta}$ and $Bi_2Sr_2CaCu_2O_{8+x}$ films is shown in Fig. 2. The Seebeck effect is measured along strip C. The strips A and B were used as thermometers for accurately determining the average temperature between the strip A and B and the temperature gradient along strip C. For measuring the Seebeck effect the applied temperature gradient was kept as small as possible in order to minimize the temperature difference between the two voltage leads. Typically, the temperature difference was less than 0.5 K and could be reduced down to less than 50 mK for high precision measurements. In our experiments the temperature gradient always was parallel and the applied field perpendicular to the Cu-O planes.

Figure 10 shows the Seebeck coefficients S_{YBCO} and S_{BSCCO} for different values of the magnetic field applied parallel to the *c* axis. Here, we have obtained S_{YBCO} and S_{BSCCC} by subtracting the thermopower S_{Cu} of the copper leads. Due to the flux pinning at low temperatures we have S_{YBCO}, $S_{BSCCO}=0$ and, hence, $S_{TC}=S_{Cu}$ allowing the measurement of S_{Cu}. The value of S_{Cu} in the narrow temperature regime above the transition temperature can be obtained by linear extrapolation. For both materials the measured thermopower becomes unmeasurably small at the same temperature as the longitudinal resistivity (compare Figs. 3 and 4). Furthermore,

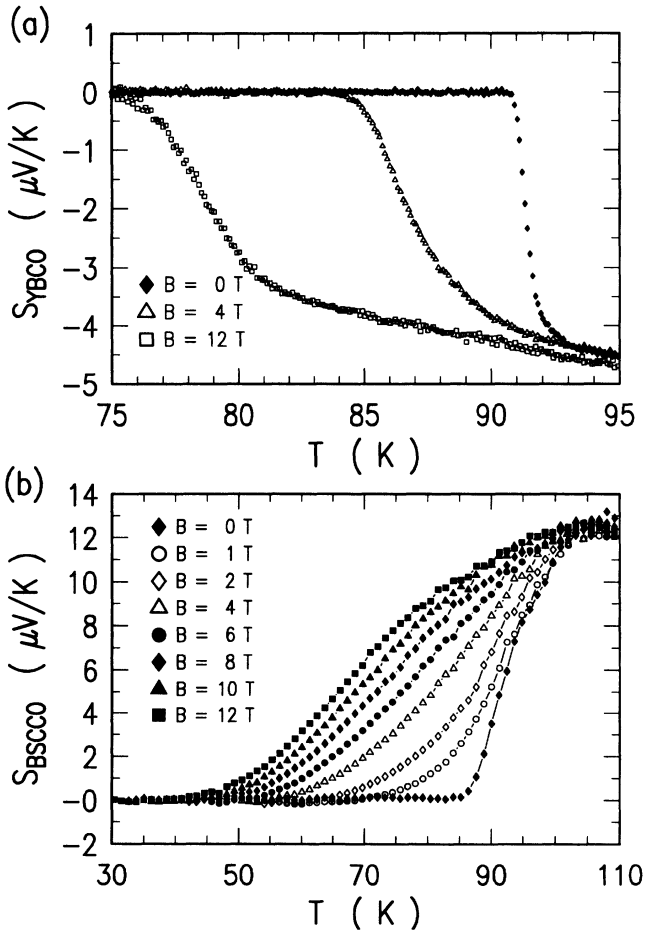

FIG. 10. Temperature dependence of the Seebeck coefficients S_{YBCO} (a) and S_{BSCCO} (b) in the mixed state of a *c*-axis-oriented $YBa_2Cu_3O_{7-\delta}$ and $Bi_2Sr_2CaCu_2O_{8+x}$ film for different magnetic fields applied in the *c* direction. The temperature gradient is applied parallel to the *ab* plane.

its temperature dependence is very similar to that of the longitudinal resistivity as expected from Eq. (17). Small deviations are caused by Hall contributions [see Eq. (21)] discussed below. This demonstrates that the Seebeck effect in the mixed state can be well described by the two-fluid counterflow picture discussed above. Howson *et al.*[106] observed a peak in the thermopower just at the zero-field transition temperature. Such peak was not observed in our experiments both for $YBa_2Cu_3O_{7-\delta}$ and $Bi_2Sr_2CaCu_2O_{8+x}$. As pointed out recently,[107] the observation of such peak can be related to the ac measuring technique used in the experiment by Howson *et al.*

The sign and the absolute magnitude of the thermoelectric power in the mixed state is determined by the normal-state thermopower. The Seebeck coefficient in the normal state sensitively depends on doping.[83–85] For the investigated $YBa_2Cu_3O_{7-\delta}$ films the thermoelectric power at the transition temperature usually ranged between -3 and -5 μV/K corresponding to $0.01<\delta<0.05$.[83] For the $Bi_2Sr_2CaCu_2O_{8+x}$ films we observed $S_n \simeq +10$ μV/K corresponding to $x \simeq 0.01$.[85] The temperature dependence of the thermopower in the mixed state is determined by the temperature dependence of the longitudinal resistivity, that is, by the flux-pinning strength of the high-T_c material. That is, the different anisotropy of $YBa_2Cu_3O_{7-\delta}$ and $Bi_2Sr_2CaCu_2O_{8+x}$ influences $S(T)$ by the different pinning behavior. The magnitude and sign of the thermopower, however, is determined by the normal-state properties of the materials. Apparently, the different anisotropy of $YBa_2Cu_3O_{7-\delta}$ and $Bi_2Sr_2CaCu_2O_{8+x}$ has only negligible influence on the normal-state thermopower for the temperature gradient applied parallel to the Cu-O planes.

C. Hall effect

In Figs. 11(a) and 11(b) we show the temperature dependence of the Hall coefficients $R_H=\rho_{xy}/H$ of $YBa_2Cu_3O_{7-\delta}$ and $Bi_2Sr_2CaCu_2O_{8+x}$, respectively, measured at different magnetic fields. The data were obtained from *c*-axis-oriented, epitaxial films with the magnetic field applied parallel to the *c* direction and the transport current density flowing in the *ab* plane. In the normal state the Hall coefficient is positive and independent of the applied field for both materials. This is, the Hall resistivity or, equivalently, the Hall tangent $\tan\theta_H$ increases linearly with the applied magnetic field as usually observed for normal metals. Figure 11 also shows that the magnitude of the normal-state Hall coefficient of $YBa_2Cu_3O_{7-\delta}$ and $Bi_2Sr_2CaCu_2O_{8+x}$ is similar. This is reasonable, since both materials have Cu-O double layers and, hence, the electric transport properties parallel to the Cu-O sheets are expected to be similar.

In the mixed state both materials show a sign anomaly of the Hall coefficient at low magnetic field just below the transition temperature. For $YBa_2Cu_3O_{7-\delta}$ the Hall coefficient becomes negative for decreasing temperature and then approaches zero. This sign anomaly is present only up to $H=6$ T, whereas for higher fields the Hall coefficient is positive over the whole temperature regime of our measurements. For $Bi_2Sr_2CaCu_2O_{8+x}$ the sign anomaly is observed only for $H<4$ T. For fields between about 2 and 3 T the Hall coefficient first becomes negative and then positive again for decreasing temperature. This double sign reversal is similar that of earlier reports on Tl-2:2:1:2 (Refs. 38 and 42) and Bi-2:2:1:2 samples.[36,46] For $H>4$ T the Hall coefficient stays positive, however, the $R_H(T)$ curves show a clear dip which becomes less pronounced for increasing magnetic field.

According to our data on the anisotropic $YBa_2Cu_3O_{7-\delta}$ and extremely anisotropic $Bi_2Sr_2CaCu_2O_{8+x}$ superconductors the observation of a second sign change in the $R_H(T)$ dependence for decreasing temperature depends on whether the pinning becomes strong enough to suppress ρ_{xy} before the second sign change occurs. The stronger pinning in $YBa_2Cu_3O_{7-\delta}$ does not allow the observation of this second sign reversal, whereas due to the small pinning in $Bi_2Sr_2CaCu_2O_{8+x}$ the double sign reversal can be observed for a certain field range. Apparently, the double sign reversal is depressed by pinning. Wang and Ting[50] have explained the sign reversal of the Hall coefficient by the pinning-induced backflow of normal carriers in the vortex core. In contrast, our experimental data suggest that the sign anomaly becomes less pronounced with increasing pinning in agreement with recent data on Tl-2:2:2:3 samples.[42] Hagen *et al.*[38] and Ferrell[49] explained

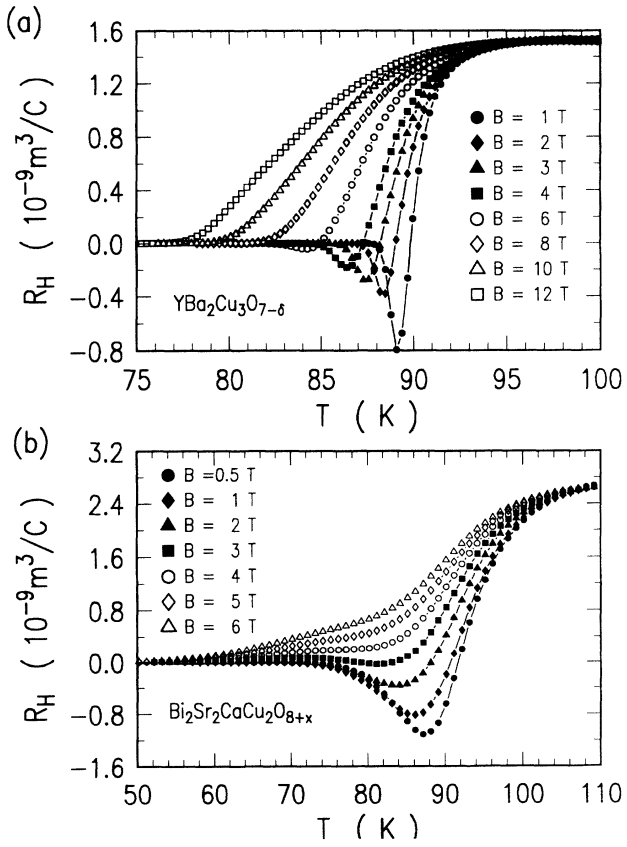

FIG. 11. Temperature dependence of the Hall coefficient R_H in the mixed state of a *c*-axis-oriented $YBa_2Cu_3O_{7-\delta}$ (a) and $Bi_2Sr_2CaCu_2O_{8+x}$ film (b) for different magnetic fields applied in the *c* direction.

the sign anomaly by the existence of an additional damping force which is proportional to the superfluid velocity v_s. Vinokur *et al.*[53] have argued against such damping force, since it would violate the dissipationless flow properties of a superfluid. As discussed above, they find $\tan\theta_H = \alpha/[\eta+\gamma(u)]$, where the sign is determined by the sign of α. Recent experiments by Harris, Ong, and Yan[40] suggest that the Hall resistivity of vortices that lie parallel to and perpendicular to the Cu-O sheets has an opposite sign. In their picture the sign anomaly of the Hall effect results from the competition between the Magnus forces acting on the interlayer segments (parallel to the Cu-O sheets) and the pancakes in a vortex line. Near T_c strong fluctuations generate a significant population of the former even for the magnetic field applied perpendicular to the Cu-O sheets.

In Figs. 12(a) and 12(b) we have plotted ρ_{xy} versus ρ_{xx} of epitaxial $YBa_2Cu_3O_{7-\delta}$ and $Bi_2Sr_2CaCu_2O_{8+x}$ films on a log-log plot for different magnetic fields. The solid lines are fits to the experimental data. Figure 12 clearly shows that for both $YBa_2Cu_3O_{7-\delta}$ and $Bi_2Sr_2CaCu_2O_{8+x}$ the low resistivity part of the curves scales to the universal power law $\rho_{xy} = K^{-1}\rho_{xx}^{\beta}$ with a coefficient K that is almost field independent. For $YBa_2Cu_3O_{7-\delta}$ and $Bi_2Sr_2CaCu_2O_{8+x}$ we have $\beta = 2.0\pm0.2$ and 1.8 ± 0.2, respectively. We note that both α and ρ_{xx} are temperature dependent. However, in the regime of thermally activated flux motion ρ_{xx} changes rapidly with temperature whereas possible changes of α are smaller. Therefore, in Eq. (18) the temperature dependence is dominated by ρ_{xx}^2. Neglecting the temperature dependence of α and assuming $\beta = 2$ the coefficient K is obtained to $K = 5.0\times10^3$ $\mu\Omega$ cm and 5.5×10^4 $\mu\Omega$ cm for $YBa_2Cu_3O_{7-\delta}$ and $Bi_2Sr_2CaCu_2O_{8+x}$, respectively. The value for $Bi_2Sr_2CaCu_2O_{8+x}$ agrees well with those derived by Samoilov[46] from measurements on $Bi_2Sr_2CaCu_2O_{8+x}$ single crystals. According to Eq. (18) the field independent value of K is equivalent to $\tan\theta_H \propto H$. This is in agreement with the Bardeen-Stephen theory where the Hall effect in the mixed state is due to the normal carrier Hall effect in the vortex cores.

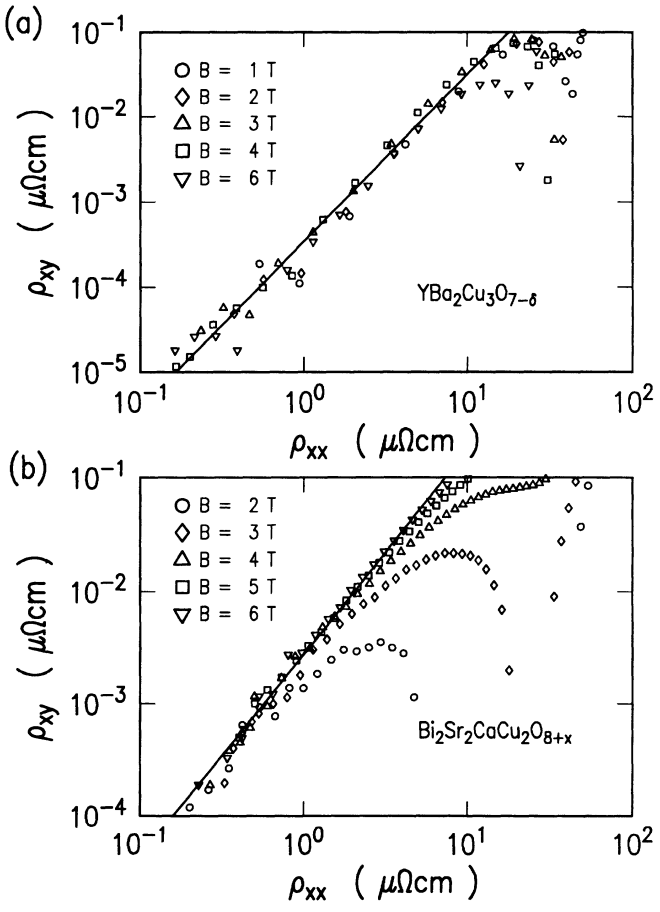

FIG. 12. ρ_{xy} versus ρ_{xx} dependences for a c-axis-oriented $YBa_2Cu_3O_{7-\delta}$ (a) and $Bi_2Sr_2CaCu_2O_{8+x}$ films (b) for different magnetic fields applied in the c direction. The solid lines are fits to the theory of Vinokur *et al.*[53]

The scaling behavior shown in Fig. 12 agrees well with the arguments of Vinokur *et al.*[53] As discussed in Sec. II C, Dorsey and Fisher[51,52] explained the same scaling behavior as a result of the glassy scaling near the vortex-glass transition in agreement with recent experiments on $YBa_2Cu_3O_{7-\delta}$ films. For $Bi_2Sr_2CaCu_2O_{8+x}$ the situation is different. Here, the quasi-2D nature of the material results in a very low glass temperature. For example, from experiments on $Bi_2Sr_2CaCu_2O_{8+x}$ single crystals a glass temperature $T_g = 20.2$ K was obtained by Safar *et al.*[108] No scaling behavior is expected according to the theory of Dorsey *et al.* at temperatures well above T_g. This is in contrast to our experimental observation and suggests that the observed scaling behavior indeed is a general feature of any vortex state with disorder dominated dynamics as proposed by Vinokur *et al.*[53]

The data shown in Figs. 11 and 12 were obtained by employing the Lorentz force of an applied transport current. Information on the Hall effect can be obtained also by measuring the longitudinal and transverse electric field due to the thermal force of an applied temperature gradient. Our experimental data were found to agree well with the predictions of Eqs. (21) and (22) as discussed in detail in Ref. 32. First, no first-order Hall contribution of the form $(S_n/\rho_n)\rho_{xy}$ to the transverse electric field $E_y/\nabla_x T$ is observed. Due to the different temperature dependence of S_ϕ and S_n such contribution should appear as a pronounced shoulder in the $E_y(T)/\nabla_x T$ curves just at the mean-field transition temperature. Because of the large value of S_n this shoulder should be observable even if the Hall tangent is smaller than 0.005. Secondly, a pronounced Hall contribution to the longitudinal electric field is observed. The derived Hall tangent ranged between 0.3 and 0.5 for $YBa_2Cu_3O_{7-\delta}$ (Ref. 32) and is by more than an order of magnitude larger than that obtained from Lorentz force measurements. Furthermore, it does not show any sign reversal.[32] A similar result is obtained for $Bi_2Sr_2CaCu_2O_{8+x}$.

As discussed in Sec. II C a possible explanation for the different Hall tangents derived from Lorentz and thermal force measurements may be the presence of vortex-antivortex pairs. Since the thermal force does not depend

on vorticity, a much larger *thermal* Hall tangent is expected, if there is a large number of free vortices and antivortices [see Eq. (23)]. However, due to the much larger anisotropy of $Bi_2Sr_2CaCu_2O_{8+x}$ as compared to $YBa_2Cu_3O_{7-\delta}$, a much stronger enhancement of the thermal Hall tangent is expected for $Bi_2Sr_2CaCu_2O_{8+x}$. This is not observed experimentally. To clarify this point a further experimental and theoretical study is required.

ACKNOWLEDGMENT

We acknowledge stimulating discussions with F. Kober and technical support by K.-H. Freudenmann, M. Kleinmann, Th. Nissel, and H.-G. Wener. This work was supported by the Bundesminister für Forschung und Technologie (project Nos. 13N5482, 13N5843, and 13N5748A).

[1]T. T. M. Palstra, B. Battlogg, L. F. Schneemeyer, R. B. van Dover, and J. V. Waszczak, Phys. Rev. B **38**, 5102 (1988); **41**, 6621 (1990); Appl. Phys. Lett. **54**, 763 (1989).

[2]P. Berghuis, P. H. Kes, B. Dam, G. M. Stollman, and J. van Bentum, Physica C **167**, 348 (1990).

[3]K. A. Müller, M. Takashige, and J. G. Bednorz, Phys. Rev. Lett. **58**, 1143 (1987).

[4]Y. Yeshurun and A. P. Malozemoff, Phys. Rev. Lett. **60**, 2202 (1988).

[5]A. P. Malozemoff, T. K. Worthington, Y. Yeshurun, F. Holtzberg, and P. H. Kes, Phys. Rev. B **38**, 7203 (1988).

[6]J. van den Berg, C. J. van der Beek, P. H. Kes, J. A. Mydosh, M. J. V. Menken, and A. A. Menovsky, Supercond. Sci. Technol. **1**, 249 (1989).

[7]Ph. Seng, R. Gross, U. Baier, M. Rupp, D. Koelle, R. P. Huebener, P. Schmitt, G. Saemann-Ischenko, and L. Schultz, Physica C **192**, 403 (1992).

[8]M. P. A. Fisher, Phys. Rev. Lett. **62**, 1415 (1989).

[9]D. R. Nelson, Phys. Rev. Lett. **60**, 1973 (1988); Phys. Rev. B **39**, 9153 (1989).

[10]M. V. Feigel'man and V. M. Vinokur, Phys. Rev. B **41**, 8986 (1990).

[11]A. Houghton, R. A. Pelcovits, and A. Sudbo, Phys. Rev. B **40**, 6763 (1989).

[12]E. H. Brandt, Phys. Rev. Lett. **63**, 1106 (1989).

[13]V. G. Kogan and L. J. Campbell, Phys. Rev. Lett. **62**, 1552 (1989).

[14]A. Sudbo and E. H. Brandt, Phys. Rev. Lett. **66**, 1781 (1991).

[15]M. V. Feigel'man, V. B. Geshkenbein, A. I. Larkin, and V. M. Vinokur, Phys. Rev. Lett. **63**, 2303 (1989).

[16]P. H. Kes, J. Aarts, J. van den Berg, C. J. van der Beek, and J. A. Mydosh, Supercond. Sci. Technol. **1**, 242 (1989).

[17]G. Blatter, V. B. Geshkenbein, and V. M. Vinokur, Phys. Rev. Lett. **66**, 3297 (1991).

[18]M. Zeh, H.-C. Ri, F. Kober, R. P. Huebener, A. V. Ustinov, J. Mannhart, R. Gross, and A. Gupta, Phys. Rev. Lett. **64**, 3195 (1990); Physica C **167**, 6 (1990).

[19]M. Galffy, A. Freimuth, and U. Murek, Phys. Rev. B **41**, 11 029 (1990); A. Freimuth, C. Hohn, and M. Galffy, *ibid.* **44**, 10 396 (1991).

[20]H. Lengfellner, A. Schnellbögel, J. Betz, W. Prettl, and K. F. Renk, Phys. Rev. B **42**, 6264 (1990).

[21]F. Kober, H.-C. Ri, R. Gross, D. Koelle, R. P. Huebener, and A. Gupta, Phys. Rev. B **44**, 11 951 (1991).

[22]M. A. Howson, M. B. Salomon, T. A. Freidmann, J. P. Rice, and D. Ginsberg, Phys. Rev. B **41**, 300 (1990).

[23]S. J. Hagen, C. J. Lobb, R. L. Greene, M. G. Forrester, and J. Talvacchio, Phys. Rev. B **42**, 6777 (1990); **43**, 6247 (1991).

[24]G. Yu. Logvenov, M. Hartmann, and R. P. Huebener, Phys. Rev. B **46**, 11 102 (1992).

[25]N. V. Zavaritsky, A. V. Samoilov, and A. A. Yurgens, Physica C **180**, 417 (1991).

[26]T. T. M. Palstra, B. Batlogg, L. F. Schneemeyer, and J. V. Waszcak, Phys. Rev. Lett. **64**, 3090 (1990).

[27]R. A. Richardson, S. D. Peacor, F. Nori, and U. Uher, Phys. Rev. Lett. **67**, 3856 (1991); see also Phys. Rev. B **44**, 9508 (1991).

[28]A. Dascoulidou, M. Galffy, C. Hohn, N. Knauf, and A. Freimuth (unpublished).

[29]H.-C. Ri, F. Kober, R. Gross, R. P. Huebener, and A. Gupta, Phys. Rev. B **43**, 13 739 (1991).

[30]V. L. Ginzburg, Zh. Eksp. Teor. Fiz. **14**, 177 (1944) [J. Phys. USSR **8**, 148 (1944)]; Usp. Fiz. Nauk **161-163**, 1 (1991) [Sov. Phys. Usp. **34**, 101 (1991)].

[31]R. P. Huebener, A. V. Ustinov, and V. K. Kaplunenko, Phys. Rev. B **42**, 4831 (1990); R. P. Huebener, Physica C **168**, 605 (1990).

[32]H.-C. Ri, F. Kober, A. Beck, L. Alff, R. Gross, and R. P. Huebener, Phys. Rev. B **47**, 12 312 (1993).

[33]A. V. Samoilov, A. A. Yurgens, and N. K. Zavaritsky, Phys. Rev. B **46**, 6643 (1992).

[34]M. Galffy and E. Zirngibl, Solid State Commun. **68**, 929 (1988).

[35]Y. Iye, S. Nakamura, and T. Tamegai, Physica C **159**, 616 (1989).

[36]S. M. Artemenko, I. E. Gorlova, and Y. I. Latyshev, Phys. Lett. A **138**, 428 (1989).

[37]T. R. Chien, T. W. Jing, N. P. Ong, and Z. Z. Wang, Phys. Rev. Lett. **66**, 3075 (1991).

[38]S. J. Hagen, C. J. Lobb, R. L. Greene, and J. H. Kang, Phys. Rev. B **41**, 11 630 (1990); **43**, 6246 (1991).

[39]S. J. Hagen, A. W. Smith, M. Rajeswari, J. L. Peng, Z. Y. Li, R. L. Greene, S. N. Mao, X. X. Xi, Qi Li, and C. J. Lobb, Phys. Rev. B **47**, 1064 (1993).

[40]J. M. Harris, N. P. Ong, and Y. F. Yan, Phys. Rev. Lett. **71**, 1455 (1993).

[41]J. P. Rice, N. Rigakis, D. M. Ginsberg, and J. M. Mochel, Phys. Rev. B **46**, 11 050 (1992).

[42]R. C. Budhani, S. H. Liou, Z. X. Cai, and Z. Wang, Phys. Rev. Lett. **71**, 621 (1993).

[43]P. J. M. Woeltgens, C. Dekker, and H. W. de Wijn, Phys. Rev. Lett. **71**, 3858 (1993).

[44]J. Luo, T. P. Orlando, J. M. Graybeal, X. D. Wu, and R. Muenchausen, Phys. Rev. Lett. **68**, 690 (1992).

[45]A. V. Samoilov (unpublished).

[46]A. V. Samoilov, Phys. Rev. Lett. **71**, 617 (1993).

[47]A. G. Aronov and S. Hikami, Phys. Rev. B **41**, 9548 (1990).

[48]R. Hopfengaertner, H. Dietrich, G. Kreiselmeyer, Ch. Müller, B. Holzapfel, and G. Saemann-Ischenko (unpublished).

[49]R. A. Ferrell, Phys. Rev. Lett. **68**, 2524 (1992).

[50]Z. I. Wang and C. S. Ting, Phys. Rev. Lett. **67**, 3618 (1991).

[51]A. T. Dorsey and M. P. A. Fisher, Phys. Rev. Lett. **68**, 694

(1992).
[52]A. T. Dorsey, Phys. Rev. B **46**, 8376 (1992).
[53]V. M. Vinokur, V. B. Geshkenbein, M. V. Feigel'man, and G. Blatter, Phys. Rev. Lett. **71**, 1242 (1993).
[54]Z. D. Wang and C. S. Ting, Phys. Rev. Lett. **69**, 1435 (1992).
[55]B. D. Josephson, Phys. Lett. **16**, 242 (1965).
[56]K. Maki, J. Low Temp. Phys. **1**, 45 (1969).
[57]C.-R. Hu, Phys. Rev. B **13**, 4780 (1976); see also **14**, 4834 (1976).
[58]A. A. Abrikosov, Zh. Eksp. Teor. Fiz. **32**, 1442 (1977) [Sov. Phys. JETP **5**, 1174 (1957)].
[59]P. G. deGennes, *Superconductivity in Metals and Alloys* (Benjamin, New York, 1966).
[60]Z. Hao, J. R. Clem, M. W. McElfresh, L. Civale, A. P. Malozemoff, and F. Holtzberg, Phys. Rev. B **43**, 2844 (1991).
[61]Z. Hao and J. R. Clem, Phys. Rev. Lett. **67**, 2371 (1991).
[62]P. Wagner, F. Hillmer, O. Frey, and H. Adrian, Phys. Rev. B **49**, 13 184 (1994).
[63]V. G. Kogan, Phys. Rev. B **24**, 1572 (1981).
[64]V. G. Kogan, N. Nakagawa, and S. L. Thiemann, Phys. Rev. B **42**, 2631 (1990).
[65]W. E. Lawrence and S. Doniach, *Proceedings of LT-12, Kyoto 1970*, edited by E. Kanda (Keigaku, Tokyo, 1970).
[66]L. N. Bulaevskii, M. Ledvij, and V. G. Kogan, Phys. Rev. B **46**, 366 (1992).
[67]L. N. Bulaevskii, M. Ledvij, and V. G. Kogan, Phys. Rev. Lett. **68**, 3773 (1992).
[68]J. R. Clem, Phys. Rev. B **43**, 7837 (1991).
[69]W. J. Skocpol and M. Tinkham, Rep. Prog. Phys. **38**, 1049 (1975).
[70]S. Ullah and A. T. Dorsey, Phys. Rev. Lett. **65**, 2066 (1990).
[71]S. Ullah and A. T. Dorsey, Phys. Rev. B **44**, 262 (1991).
[72]P. A. Lee and S. R. Shenoy, Phys. Rev. Lett. **28**, 1025 (1972).
[73]U. Welp, S. Fleshler, W. K. Kwok, R. A. Klemm, V. M. Vinokur, J. Downey, B. Veal, and G. W. Crabtree, Phys. Rev. Lett. **67**, 3180 (1991).
[74]Q. Li, M. Suenaga, T. Hikata, and K. Sato, Phys. Rev. B **46**, 5857 (1992).
[75]Q. Li, K. Shibutani, M. Suenaga, I. Shigaki, and R. Ogawa, Phys. Rev. B **48**, 9877 (1993).
[76]Q. Li, M. Suenaga, L. Bulaevskii, T. Hikata, and K. Sato (unpublished).
[77]U. Welp, S. Fleshler, W. K. Kwok, R. A. Klemm, V. M. Vinokur, J. Downey, B. Veal, and G. W. Crabtree, Phys. Rev. Lett. **69**, 1623 (1992).
[78]Z. Tesanovic, L. Xing, L. Bulaevskii, Q. Li, and M. Suenaga, Phys. Rev. Lett. **69**, 3563 (1992).
[79]M. B. Salamon and Jing Shi, Phys. Rev. Lett. **69**, 1622 (1992).
[80]M. B. Salamon, W. Lee, K. Ghiron, J. Shi, N. Overend, and M. A. Howson (unpublished).
[81]P. Nozieres and W. F. Vinen, Philos. Mag. **14**, 667 (1966).
[82]M. Tinkham, *Introduction to Superconductivity* (McGraw-Hill, New York, 1975).
[83]P. J. Ouseph and M. Ray O'Bryan, Phys. Rev. B **41**, 4123 (1990).
[84]J. R. Cooper, S. D. Obertelli, A. Carrington, and J. W. Loram, Phys. Rev. B **44**, 12 086 (1991).
[85]S. D. Obertelli, J. R. Cooper, and J. L. Tallon, Phys. Rev. B **46**, 14 928 (1992).
[86]H. Lengfellner, G. Kremb, A. Schnellbögl, J. Betz, K. F. Renk, and W. Prettl, Appl. Phys. Lett. **60**, 501 (1992).
[87]J. Bardeen and M. J. Stephen, Phys. Rev. **140**, A1197 (1965).
[88]K. Maki, Prog. Theor. Phys. **41**, 902 (1982); J. Low Temp. Phys. **1**, 45 (1969).
[89]J. M. Kosterlitz and D. J. Thouless, J. Phys. C **6**, 1181 (1973); see also J. M. Kosterlitz, *ibid.* **7**, 1046 (1973).
[90]P. Minnhagen, Rev. Mod. Phys. **59**, 1001 (1987).
[91]S. Martin, A. T. Fiory, R. M. Fleming, G. P. Espinosa, and A. S. Cooper, Phys. Rev. Lett. **62**, 677 (1989).
[92]N. C. Yeh and C. C. Tsuei, Phys. Rev. B **39**, 9708 (1989).
[93]R. Gross, H.-C. Ri, F. Gollnik, and R. P. Huebener, Physica B **194-196**, 1365 (1994).
[94]Y. Matsuda, S. Komiyama, T. Terashima, K. Shimura, and Y. Bando, Phys. Rev. Lett. **69**, 3228 (1992).
[95]A. V. Samoilov, Phys. Rev. B **49**, 1246 (1994).
[96]N. B. Kopnin, B. I. Ivlev, and V. A. Kalatsky, Pis'ma Zh. Eksp. Teor. Fiz. **55**, 717 (1992) [JETP Lett. **55**, 750 (1992)].
[97]A. G. Aronov and A. B. Rapoport, Mod. Phys. Lett. B **6**, 1083 (1992).
[98]P. Wagner, H. Adrian, and C. Tome Rosa, Physica C **195**, 258 (1992).
[99]P. Wagner, F. Hiller, U. Frey, H. Adrian, T. Steinborn, L. Ranno, A. Elschner, I. Heyvaert, and Y. Bruynseraede, Physica C **215**, 123 (1993).
[100]L. Alff, G. M. Fischer, R. Gross, F. Kober, A. Beck, K.-D. Husemann, T. Nissel, F. Schmidl, and C. Burckhardt, Physica C **200**, 277 (1992).
[101]J. Gohng and D. K. Finnemore, Phys. Rev. B **46**, 398 (1992).
[102]J. R. Clem, Ann. Phys. Rev. (N.Y.) **40**, 268 (1966).
[103]N. R. Werthamer, E. Helfand, and P. C. Hohenberg, Phys. Rev. **147**, 295 (1966).
[104]Q. Li, M. Suenaga, J. Gohng, D. K. Finnemore, T. Hikata, and K. Sato, Phys. Rev. B **46**, 3195 (1992).
[105]F. Gollnik, R. Gross, H.-C. Ri, and R. P. Huebener (unpublished).
[106]M. A. Howson, M. B. Salomon, T. A. Friedmann, J. P. Rice, and D. Ginsberg, Phys. Rev. B **44**, 9757 (1990).
[107]G. Yu. Logvenov, V. V. Ryazanov, R. Gross, and F. Kober, Phys. Rev. B **47**, 15 322 (1993).
[108]H. Safar, P. L. Gammel, D. J. Bishop, D. B. Mitzi, and A. Kapitulnik, Phys. Rev. Lett. **68**, 26 722 (1992).

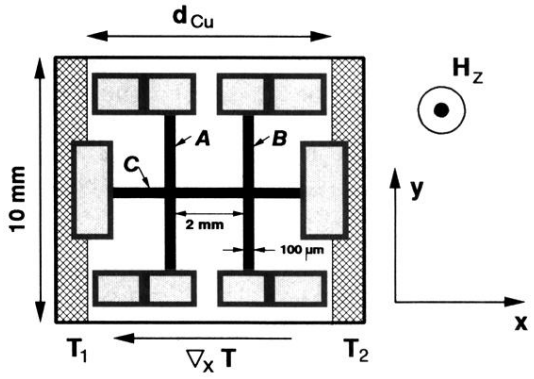

FIG. 2. Sketch of the thin-film sample configuration used in our experiments. The Nernst effect is measured either with strip A or B, whereas the Seebeck effect is measured with strip C. The hatched area indicates the substrate part that are glued onto the copper blocks which are kept at different temperatures in order to establish a temperature gradient along the x direction.